Economic Geology, v. 116, no. 7, pp. 1537–1560

The Source of Organic Matter and Its Role in Producing Reduced Sulfur for the Giant Sediment-Hosted Jinding Zinc-Lead Deposit, Lanping Basin, Yunnan, Southwest China

Qing Lan,[1] Ruizhong Hu,[1,2,†] Xianwu Bi,[1] Hu Liu,[3] Jiafei Xiao,[1] Shanling Fu,[1] M. Santosh,[4,5] and Yongyong Tang[1]

[1]*State Key Laboratory of Ore Deposit Geochemistry, Institute of Geochemistry, Chinese Academy of Sciences, Guiyang 550081, China*

[2]*College of Earth and Planetary Sciences, University of Chinese Academy of Sciences, Beijing 100049, China*

[3]*Sichuan Key Laboratory of Shale Gas Evaluation and Exploitation, Chengdu 610091, China*

[4]*School of Earth Sciences and Resources, China University of Geosciences Beijing, 29 Xueyuan Road, Beijing 100083, China*

[5]*Department of Earth Sciences, University of Adelaide, SA 5005, Australia*

Abstract

The Jinding deposit, located in the northern part of Lanping basin in southwest China, is the second largest Zn-Pb deposit in China and the third largest Mississippi Valley-type deposit identified globally. The deposit consists of several large tabular orebodies within the Jinding dome. Two stages of sulfide mineralization (sphalerite, galena, and pyrite) are identified, which are mainly hosted in the siliciclastic strata of Early Cretaceous and Paleocene age. The early sulfide minerals are mostly fine grained (<100 μm) and disseminated in the host rocks, whereas the late minerals are ty pically coarse grained (up to 1 mm in diameter) and colloform. It is estimated that about 3.17×10^6 m^3 of reduced sulfur (H_2S) was involved in the sulfide mineralization of the Jinding deposit, although its origin remains equivocal. Here, we investigate the biomarker signatures of organic matter and the mechanism of generation of the H_2S. The organic matter in the Jinding deposit occurs mainly as petroleum filling fractures and cavities in the wall rocks and solid bitumen intergrown with sulfides or calcite. Abundant solid bitumen is also found on the surfaces of the carbonate rocks in the Sanhedong Formation as well as in the rock fractures associated with framboidal pyrite. The petrographic characteristics and maturity-related biomarker parameters show that the solid bitumen in the ores has higher thermal maturity than that in the Sanhedong Formation, suggesting that it was generated at different temperatures in the two settings. The source-related parameters suggest that the solid bitumen in the ores and Sanhedong Formation probably both originated in a mixed marine shale and carbonate environment and that the source rocks for the bitumen precursor were late Triassic marine strata.

The $\delta^{34}S$ values, ranging from –30 to –10‰ for the fine-grained and disseminated sulfide minerals and from –24.50 to –16.27‰ for the solid bitumen in the early (main) mineralization stage, suggest that H_2S was generated by microbial sulfate reduction. We propose that this occurred in the Triassic strata prior to or during migration of hydrocarbons to the Jinding dome to form a H_2S-enriched paleo-oil reservoir. This hypothesis is supported by the similarity of the $\delta^{34}S$ values (–27.62 to –17.38‰) of solid bitumen in the Sanhedong Formation (the source rocks) to that of bitumen in the ores. The late-ore sulfide, however, displays significantly higher $\delta^{34}S$ values, ranging from –8 to 0‰. We propose that the H_2S of this stage was mainly generated by thermochemical sulfate reduction as a result of the interaction between hydrocarbons, sulfate, and hydrothermal fluid. The hydrocarbons were oxidized into bitumen that has $\delta^{34}S$ values from –7.38 to –4.61‰.

Introduction

The association of organic matter with sulfide mineralization has been reported for a variety of ore deposit types that contain metals such as Cu, U, Pb, and Zn (Powell and Macqueen, 1984; Kesler et al., 1994; Cisternas and Hermosilla, 2006; Wilson et al., 2007). However, the association between organic matter and ore is still not completely understood (Spangenberg and Macko, 1998; Saintilan et al., 2015; Rybicki et al., 2017). In many cases, hydrocarbons migrate separately from or together with the mineralizing fluids within sedimentary basins and deposit in the form of petroleum or solid bitumen in the vicinity of sulfides (Püttmann et al., 1988; Manning and Gize, 1993; Kozłowski, 1995; Spangenberg and Herlec, 2006; Rieger et al., 2008; Williford et al., 2011). Examples include the stratabound Cu deposits in Chile (Rieger et al., 2008), the Athabasca U deposits in Canada (Wilson et al., 2007), and some Zn-Pb deposits (Rybicki et al., 2017). A detailed characterization of the organic matter associated with such ore deposits, including source and thermal maturity traced using biomarker parameters, would aid in understanding the link between organic matter and ore deposition (Rybicki et al., 2017). Organic matter can be involved in the generation of reduced sulfur (H_2S), acting as a reducing agent either through microbial sulfate reduction (MSR), also referred to as bacterial sulfate reduction or abiological thermochemical sulfate reduction (TSR), leading to base metal sulfide deposition (Powell and Macqueen, 1984; Leventhal, 1990). As MSR produces more depleted ^{34}S than TSR during the transformation of sulfates to sulfides (Brunner and Bernasconi, 2005; Johnston et al., 2007; Canfield et al., 2010; Sim et al., 2011), the $\delta^{34}S$ value of H_2S can be used to differentiate between these two processes.

The Jinding deposit, located in the northern part of Lanping basin in Yunnan, southwest China, has a proven reserve of 220 Mt of ore that contains 6.1% Zn and 1.3% Pb and covers a sur-

†Corresponding author: e-mail, huruizhong@vip.gyig.ac.cn

 Submitted: August 17, 2020 / Accepted: January 25, 2021

face area of about 8 km² (Third Geological Team, 1984; Xue et al., 2007a). It is the second largest Zn-Pb deposit in China and the third largest Mississippi Valley-type (MVT) deposit identified to date (Leach and Song, 2019; Song et al., 2019) (Fig. 1). The ongoing mining in this deposit has revealed abundant oil and solid bitumen closely associated with the ores, and previous studies have speculated that they played an important role in the precipitation of Zn and Pb sulfides in this deposit (Hu, 1989; Fu et al., 2006; Xue et al., 2007b; Gao et al., 2012). Consequently, the Jinding deposit is the ideal place in which to investigate the detailed metallogenic processes that involve organic matter.

The deposit is mainly concentrated in the Jinding dome as tabular orebodies hosted in siliciclastic strata of Early Cretaceous and Paleocene age. The genesis of the Jinding deposit has long been debated. The diverse genetic models proposed in previous studies for this deposit include (1) a syngenetic origin (Qin and Zhu, 1991; Luo et al., 1994; Hu et al., 1998), (2)ban epigenetic origin that involved postsedimentary hydrothermal deposition or modification of earlier sulfides (Kyle and Li, 2002; Xue et al., 2007a), and (3) MVT-style mineralization in a diapiric setting (Wang et al., 2009; Leach et al., 2016; Leach and Song, 2019; Song et al., 2020). Although many questions remain unanswered regarding the mechanism and environment of mineralization, the epigenetic and diapir-related origin are favored over a syngenetic origin because the orebodies occur in sandstones of the lower Cretaceous Jingxing Formation as well as in the sandstones and conglomerates of the Paleocene Yunlong Formation, which are separated by a thrust fault (Kyle and Li, 2002; Xue et al., 2007a; Leach et al., 2016; Song et al., 2020). The metallogenetic epoch of the Jinding deposit remains poorly constrained, but the regional geologic features and thermochronological data indicate that the Zn-Pb mineralization in this deposit was generated during

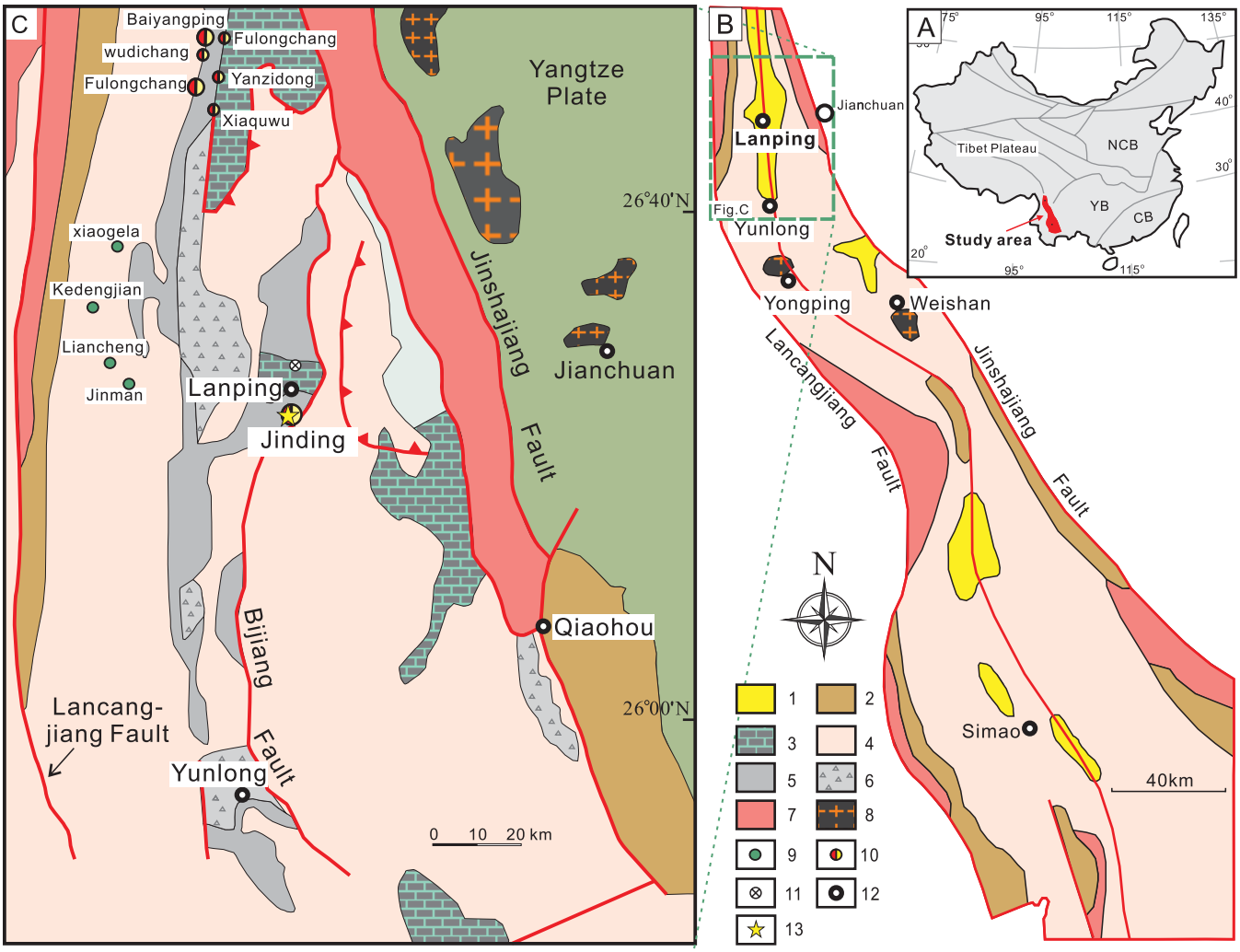

Fig. 1. (A-C) Simplified geologic map of the Lanping-Simao basin in western Yunnan, China, showing the major structural features and the location of the Jinding deposit (modified after Xue et al., 2007a). 1 = Cenozoic sandstone, breccia, siltstone, mudstone rocks, and gypsums, 2 = pre-Mesozoic metamorphic rocks, 3 = Upper Triassic limestone, 4 = Jurassic to Cretaceous clastic rocks, 5 = Paleocene sandstone and siltstone, 6 = Eocene breccia and sandstone, 7 = Middle-Upper Triassic volcanic rocks, 8 = Himalayan intrusions, 9 = Cu mineralized zone, 10 = Pb-Zn mineralized zone, 11 = sampling location for the samples outside the metallogenic region, 12 = city, 13 = study area: the giant Jinding deposit. CB = Cathaysia block, NCB = North China block, YB = Yangtze block.

the Oligocene to Miocene (apatite fission track age of 32 to 21 Ma; Li and Song, 2006; Wang et al., 2009), associated with the large-scale regional hydrothermal activity during a late stage (41–26 Ma) of the India-Asia collision (Hou et al., 2006).

It has been estimated that about 3.17×10^6 m^3 H_2S was required to form the giant Jinding Zn-Pb deposit (Gao et al., 2008). Previous studies have concluded that the H_2S was produced by MSR based on the low $\delta^{34}S$ values (Tang et al., 2014; Xue et al., 2015). However, whether the MSR process took place at the site of mineralization or in a distal area and the H_2S was transported to the site of mineralization remains unclear. It is also unknown whether the TSR occurred or how the MSR and/or TSR controlled the mineralization process in the Jinding deposit.

In this study, we characterize the solid bitumen in the Jinding deposit and Triassic Sanhedong Formation and evaluate its source and degree of thermal evolution. In addition, based on a comprehensive study of the mineralogy, including its paragenesis, the sulfur isotope composition, and the organic and inorganic geochemistry and in conjunction with published data, we discuss the source of organic matter and its role in the Zn-Pb mineralization. We also evaluate the mechanism of generation of H_2S during the different stages of mineralization and propose a new genetic model for the Jinding deposit. Our study provides insights into the evolution of fluids associated with hydrocarbons in sedimentary basins during the formation of Zn-Pb deposits.

Regional Geologic Setting of the Lanping Basin

The Sanjiang region covers the southeastern part of the Tibet Plateau and western Yunnan province in China (Fig. 1A, B). It was assembled through closure of the Paleotethyan ocean and the subsequent amalgamation of Gondwana-derived microcontinental blocks with arc terranes (Metcalfe, 2013; Deng et al., 2014). Mesozoic continental basins, including the Changdu basin in the eastern Qiangtang block and the Lanping-Simao basins in the Simao block (Fig. 1B), were developed during the amalgamation process. During the Cenozoic, continental collision and distal oceanic plate subduction largely reshaped the lithospheric structure in the Sanjiang region (Deng et al., 2014; Hou et al., 2015; Wang et al., 2016). Numerous ore deposits of diverse genetic types and metal endowment, including Cu, Zn-Pb, Au, and Mo, formed in the Cenozoic, making the Sanjiang region one of the most productive in China (Deng et al., 2012).

The Lanping basin in the central part of the Sanjiang region underwent a complex evolutionary process from a remnant marine basin and continental depression basin during the Mesozoic to a pull-apart continental basin during the Cenozoic (Xue et al., 2002). There are three major NNW-trending regional faults in the basin, namely, the Jinshajiang-Ailaoshan and Lancangjiang faults along the eastern and western margins of the basin and the Bijiang fault in the center of the basin (Fig. 1B, C). Geophysical and remote sensing data suggest that the faults cut through the lower crust (Yin et al., 1990; Xue et al., 2002; Jin et al., 2003). Cenozoic tectonic and igneous activity may have provided conduits and the driving force, respectively, for the fluids in the basin, thereby contributing in an important way to the formation of the deposits (Zhang et al., 2000; Xue et al., 2002, 2003).

Precambrian and Paleozoic rocks are mainly distributed along the margins of the Lanping basin. Mesozoic and Cenozoic strata, which are more than 10 km thick, are exposed inside the basin. The oldest of them are Upper Triassic strata that occur in the central part of the basin and include the Waigucun Formation (T_3w), Sanhedong Formation (T_3s), Waluba Formation (T_3wl), and Maichujing Formation (T_3m) (Fig. 2A), which were deposited in a marine or marine-terrigenous environment. Among them, the Sanhedong Formation (T_3s) is the only one that contains marine carbonate rocks. This formation is composed mainly of limestone, dolomite limestone, bioclastic limestone, and marl, all of which were deposited on a carbonate platform. Owing to a gradual uplift, the basin was filled with a series of Jurassic to Cretaceous continental clastic sequences (Fig. 2A). The Cenozoic sequences are composed mainly of reddish continental clastic rocks; several evaporite layers are present (Fig. 2A; Third Geological Team, 1984). There is a marked unconformity between the Cretaceous and Paleogene formations (Fig. 2A; Xue et al., 2002). Some strata within the basin have been folded and faulted, but not regionally metamorphosed, and were locally intruded by Himalayan alkaline magmatic bodies such as the Zaojiaochang and Xiquechang intrusions in Yunlong County and the Zhuopan and Huanglianpu intrusions in Yongping County (Zhang et al., 2000; Xue et al., 2003; Liu et al., 2006).

More than 100 Pb-Zn-Ag-Cu deposits or occurrences have been found in the Lanping basin, most of which are concentrated in the northern segment of the basin (Fig. 1C). These deposits are commonly hosted in the Mesozoic-Cenozoic siliciclastic strata and controlled by Cenozoic thrust faults (Hou et al., 2006; He et al., 2009). The Zn-Pb deposits were mainly formed by basinal brine-dominated fluids driven by orogenic uplift as well as tectonic compression during late collisional tectonism and contemporaneous magmatism, which provided the heat sources and ore materials (Bi et al., 2019).

Geology of the Jinding Zn-Pb Deposit

The Jinding area records a complex geologic history (Third Geological Team, 1984; Kyle and Li, 2002; Xue et al., 2015). Nappe structures produced by regional westward overthrusting and a dome generated by uplift are the most conspicuous structural features in the Jinding ore district (Fig. 2B). The Jinding dome, roughly oval in shape (about 3 km long and 2.5 km wide with a NNE-trending axis), was created by the diapiric migration of late Triassic evaporites during Paleocene thrust loading (Song et al., 2020), which resulted in the Mesozoic sequences being overturned and directly overlapping the Paleocene Yunlong Formation (Fig. 2B; Wu and Wu, 1989; Song et al., 2020). As a result of the doming, the strata and faults display a radiating pattern from the center to periphery (Fig. 2B). The Jinding deposit occurs mainly as tabular orebodies in the dome.

The wall rocks of the Jinding deposit mainly comprise breccia-bearing sandstones of the Paleocene Yunlong Formation (autochthonous) and overlying sandstones of the Early Cretaceous Jingxing Formation (allochthonous). The sandstone of the Jingxing Formation is composed mainly of quartz and siliceous lithic fragments. The cements are generally carbonate (mainly calcite) but include some argillaceous material and were partially or almost entirely replaced by sulfides (e.g., py-

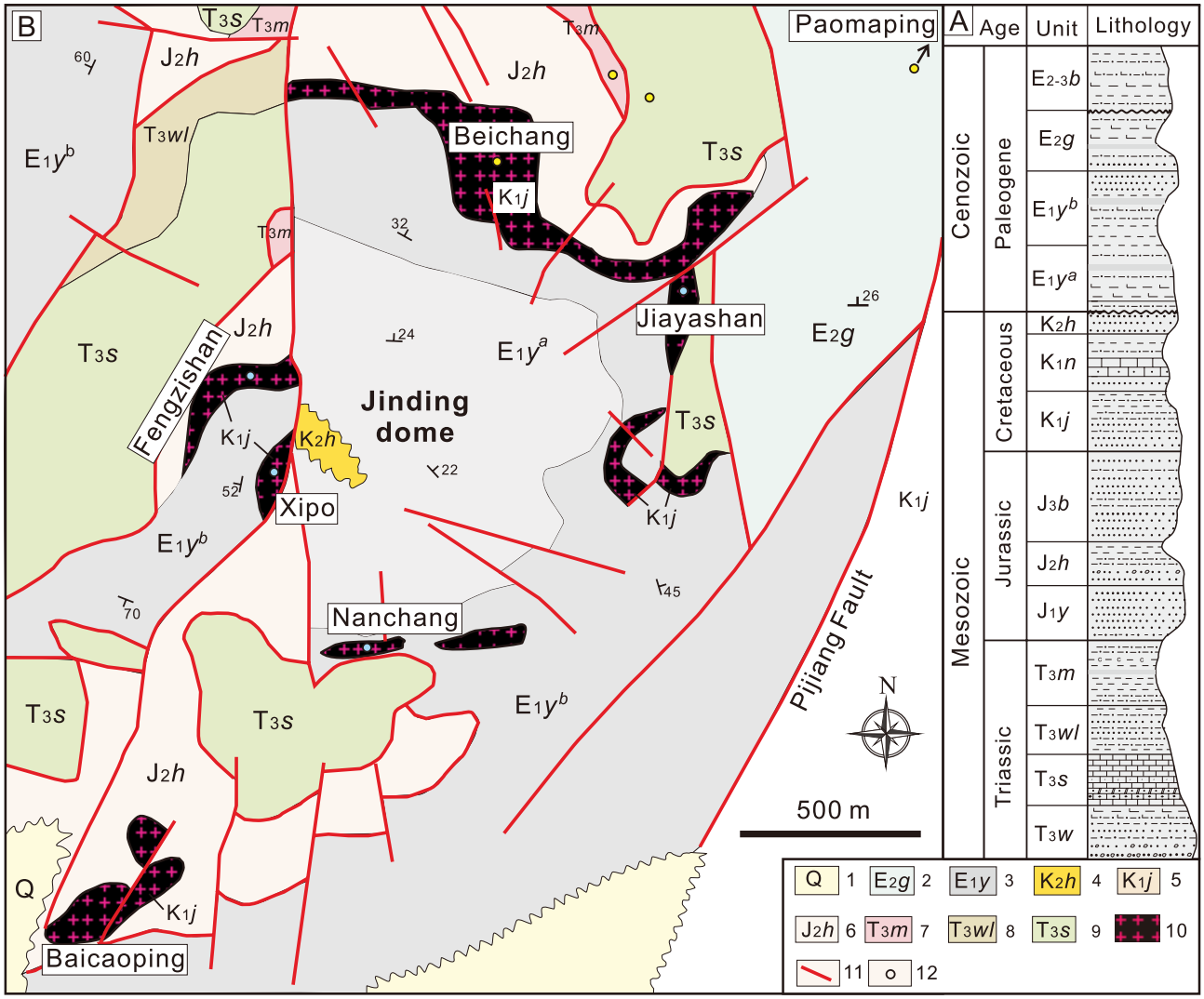

Fig. 2. A. Simplified stratigraphic column of the Lanping basin. B. Geologic and structural map of the Jinding Zn-Pb deposit (modified after Third Geological Team, 1984). 1-Q = Quaternary sediments, 2-E_2g = Eocene Guolang Formation, 3-E_1y = Paleocene Yunlong Formation, 4-K_2h = middle Cretaceous Hutoushi Formation, 5-K_1j = Lower Cretaceous Jingxing Formation, 6-J_2h = Middle Jurassic Huakaizuo Formation, 7-T_3m = Upper Triassic Maichujing Formation, 8-T_3wl = Upper Triassic Waluba Formation, 9-T_3s = Upper Triassic Sanhedong Formation, 10 = orebody, 11 = fault, 12 = sampling locations, yellow-filled circles represent sample in this study, blue denotes samples from previous studies. Samples from outside the metallogenic region are shown in Figure 1.

rite, sphalerite, galena) (Fig. 3A, B). The Yunlong Formation is composed of breccias, sandstone, and gypsum in the upper part and siltstone, mudstone, and gypsum in the lower part, that contain *Djungarica* sp. The breccia fragments are poorly rounded and sorted and consist mainly of bitumen-bearing limestone that is similar to the limestone of the Upper Triassic Sanhedong Formation (Fig. 3C, D; Xue et al., 2007a).

The Jinding deposit contains more than 100 orebodies that are grouped into seven ore blocks surrounding the core of the Jinding dome. These are the Paomaping, Beichang, Jiayashan, Fengzishan, Nanchang, Xipo, and Baicaoping ore blocks (Fig. 2B) and are possible segments of original orebodies cut by radial faults. Among them, the Beichang block is the most important one, accounting for 75% of the total reserve of the Jinding ore deposit (Third Geological Team, 1984; Xue et al., 2007a).

The orebodies in the upper part of the deposit are generally tabular or stratiform in shape. This style of mineralization is referred to as sandstone type as it is restricted to a sandstone layer (K_1j) (Fig. 3A, B). The No. 1 orebody in the Beichang ore block is the largest orebody, accounting for 60% of the total reserve of the Jinding deposit. The cap rock of the No. 1 orebody consists of siltstone and mudstone sequences of the middle Jurassic Huakaizuo Formation (J_2h), which is rich in argillaceous material and has a low permeability. The mineralization in the lower part of the orebody is referred to as breccia type because it occurs mainly in breccias of the Yunlong Formation and the bodies of ores are variable in shape, occurring as lenses, veins, and irregular bodies (Fig. 3C, D; Third Geological Team, 1984; Qin and Zhu, 1991).

The most common minerals in the primary ores are sulfides (sphalerite, galena and pyrite). The sulfide minerals are

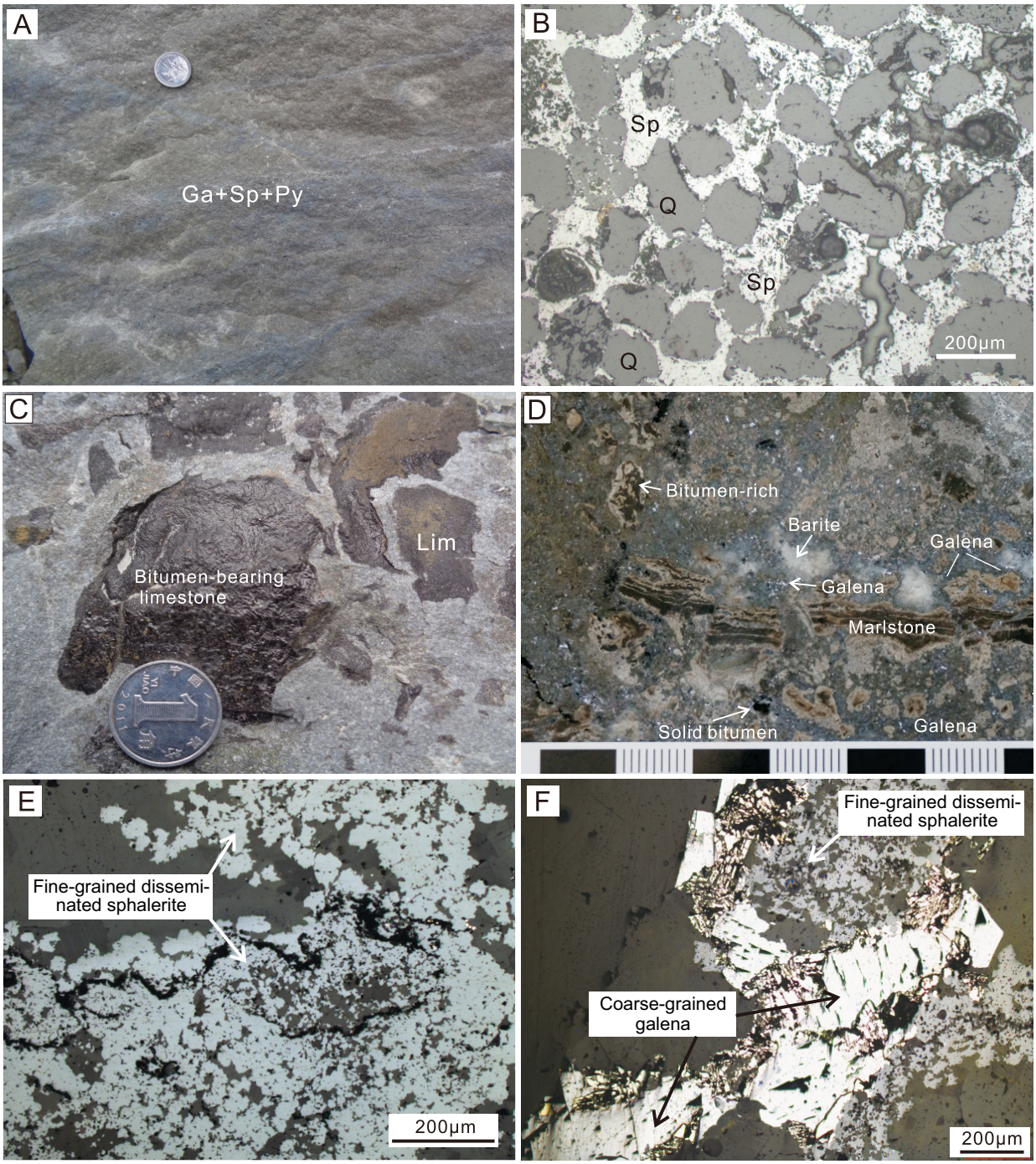

Fig. 3. Major types of mineralization in the Jinding Zn-Pb deposit. A. Sandstone-type ore showing that the disseminated sulfides of the early mineralization stage are crosscut by a late galena vein. B. Photomicrograph showing the host sandstone. The cements have been partially or almost entirely replaced by sulfides (e.g., pyrite, sphalerite, galena). C. The breccia with bitumen-bearing limestone. D. The breccia-type ore with marlstone breccia and solid bitumen. E. Fine-grained early disseminated sphalerite. F. Early fine-grained and disseminated sphalerite and late coarse-grained galena. Abbreviations: Ga = galena, Lim = limestone breccias, Py = pyrite, Q = quartz, Sp = sphalerite.

mostly fine grained (<100 μm) (Fig. 3E), but coarse-grained and colloform sulfides (up to 1 mm) are locally associated with calcite in the late-stage veins (Fig. 3F). The gangue minerals are mainly quartz, calcite, celestine, bitumen, gypsum, and barite. The sulfide mineralization has been grouped into two stages based on mineral textural relationships (Fig. 4). The earlier (main) stage is characterized by fine-grained and disseminated sulfide minerals occurring in sandstones and massive sulfide mineralization or vein mineralization in limestone breccias (Fig. 3B). In contrast, the late mineralization mainly formed coarse-grained and colloform galena and sphalerite veins (Fig. 3E), with sphalerite being less abundant than ga-

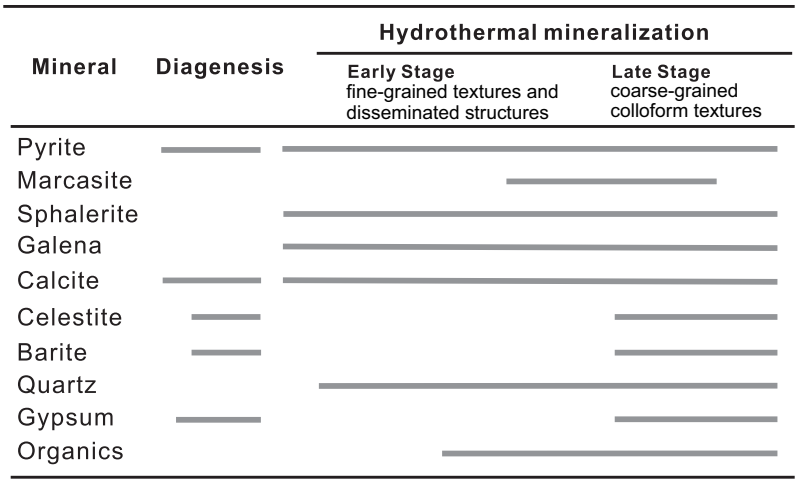

Fig. 4. Simplified paragenesis of major ore and gangue minerals in the Jinding deposit.

lena. Pyrite occurs in both stages but is more common in the late stage (Fig. 4; Xue et al., 2007a). Quartz cemented part of the ore, indicating that there was probably dissolution of detrital quartz and redeposition during a mineralization event. Sulfate minerals (including gypsum, barite, and celestine) are also widely distributed in the Jinding area (Fig. 5).

Fluid inclusions in quartz and sphalerite from the Jinding deposit show homogenization temperatures that range from 115° to 234°C (with an average of 154°C in sphalerite and from 157° to 250°C with an average of 182°C in quartz). The average salinity is 8.7 wt % NaCl equiv for fluid inclusions in quartz and 10.5 wt % NaCl equiv in sphalerite (Xue et al., 2007a; Zeng, 2007). Hydrocarbon inclusions commonly occur in sphalerite and the gangue minerals (Xue et al., 2009, Chi et al., 2017).

Sampling and Analytical Methods

Eleven solid bitumen samples were selected from the ores and the Sanhedong Formation. In order to identify the potential source rocks for the bitumen, 10 organic-rich rock samples from the wall rock and the Triassic strata in the Jinding ore field were also sampled (Fig. 2). In addition, two samples from the Triassic Sanhedong Formation located about 15 km to the north of the Jinding deposit and outside the ore district were also collected (Fig. 1). The samples were cleaned, crushed, powdered, and sieved to a obtain a <75 μm fraction. Caution was used to ensure that no samples were contaminated or that material was not lost in the operation. The soluble organic matter was extracted from the solid bitumens and powdered rock samples using chloroform at 85°C. The extracts were

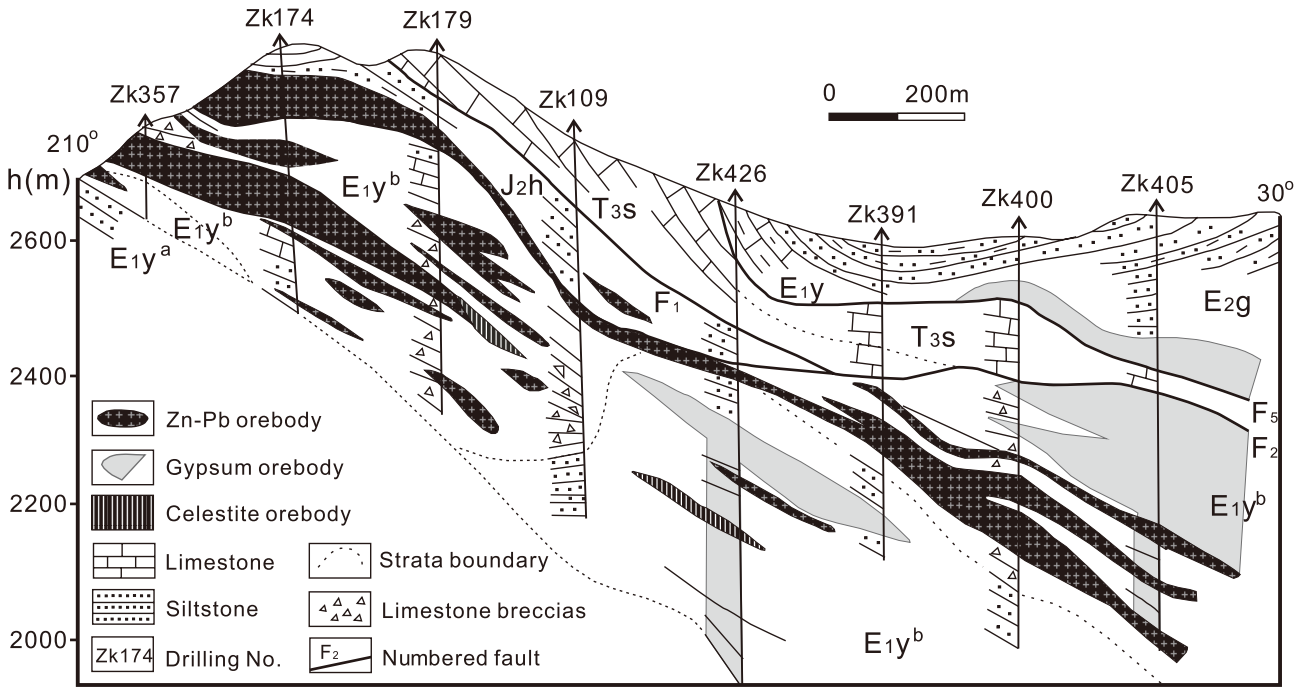

Fig. 5. Geologic section of Beichang-Paomaping ore blocks in the Jinding Zn-Pb deposit showing gypsum and celestite orebodies coexisting with Zn-Pb mineralization (modified after Third Geological Team, 1984). The stratigraphic notations are the same as those in Figure 2.

separated by mixed-bed silica-alumina liquid chromatography into fractions comprising saturated hydrocarbons, aromatic hydrocarbons, and organic compounds that contain nitrogen, sulfur, and oxygen. Gas chromatographic analysis of the saturated and aromatic fractions was performed using an Agilent 7890 gas chromatograph (GC) equipped with a DB-5 elastic quartz capillary column (length, 30 m and inner diameter, 0.25 mm) and hydrogen flame ionization detector (FID). Gas chromatographic-mass spectrometric (GC-MS) analyses were carried out using Thermo-Trace GC and Ultra-DSQII MS instruments (version, 08070173). The chromatographic column was an HP-5MS elastic quartz capillary column (60 m × 0.25 mm × 0.25 mm), and the carrier gas was helium. The initial temperature was kept at 100°C for 5 min, increased to 220°C at a rate of 4°C/min, continued to 320°C at a rate of 2°C/min, and then maintained for 20 min. These procedures were performed at the Petroleum Geology Research and Laboratory Center, Research Institute of Petroleum Exploration and Development of China, Beijing.

The methods for the separation and $\delta^{34}S$ measurement of solid bitumen were those described by Cai et al. (2017). The solid bitumen was treated with hot 6*N* HCl, a mixture of 6*N* HCl and 40% HF, and then 6*N* HCl to dissolve the minerals. Any remaining pyrite was removed from the solid bitumen by adding a mixture of hot 6*N* HCl and $CrCl_2$ under N_2 with a gas flow carrying the H_2S to a trap where it was recovered as Ag_2S. After dilution with distilled water and centrifugation, the remaining solid bitumen was separated from the residue (precipitate) using heavy liquids (KBr + ZnBr) with a density of 1.8–1.9 g/cm^3 and of 2.0–2.1 g/cm^3. The solid bitumen was collected and reground to expose new pyrite surfaces; the procedure was repeated one more time. After two treatments, the solid bitumen was analyzed using X-ray diffraction (XRD) to determine whether pyrite was below the detection limits (≤0.5%). If not, additional treatments were performed.

Following the above treatment, a known amount of solid bitumen was combusted in a Parr bomb at ca. 25 atm O_2 to oxidize organically bound sulfide to sulfate. The dissolved sulfate was precipitated as $BaSO_4$ and weighed to provide a total bitumen sulfur content. The $BaSO_4$ was weighed into a tin capsule, and $\delta^{34}S$ was determined with an elemental analyzer combustion continuous flow isotope ratio mass spectrometer (EAIsoPrime, Euro 3000, GV Instruments, United Kingdom). The standard deviation for the $\delta^{34}S$ analysis of NBS127 (barium sulfate, $\delta^{34}S$ = +20.3%) was better than ±0.2% (n = 5). Dissolved iron was measured at pH <2 using an atomic absorption spectrometer, to determine the maximum residual pyrite content in the solid bitumen after chromium reduction (assuming that all Fe occurred as pyrite in the solid bitumen). The organic sulfur content was calculated by subtracting the pyrite sulfur from the total residual solid bitumen sulfur. The isotope results are presented as $\delta^{34}S$ values relative to the Vienna Canyon Diablo Troilite standard.

Results

Occurrence of organic matter in the Jinding deposit

Organic matter is widely distributed in the Jinding deposit and occurs mainly as bitumen and crude oil filling fractures and dissolution cavities in the ores and wall rocks. It is also present as hydrocarbon inclusions in transparent and nontransparent minerals (Fig. 6; Xue et al., 2007b, 2009; Chi et al., 2017). According to its appearance and form, the organic matter was grouped into the following two categories.

The first category is organic matter on the surface of wall rocks with the strong smell of petroleum after hammering or that accumulated in cavities and fissures. Often, oil was observed to flow out from a cavity onto the fresh rock surface (Fig. 6A). Small calcite crystals were present on the sides of the cavities that contain oil and bitumen (Fig. 6B). These features indicate that paleo-oil reservoirs were very likely present at the site of the Jinding deposit before and/or during mineralization (Xue et al., 2007b, 2009; Chi et al., 2017; Song et al., 2020).

The second category comprises vein or tabularlike solid bitumen that was obviously affected by thermal alteration. This type of solid bitumen is usually intergrown with Zn and Pb sulfides and calcite, crystals of which locally approach 1 cm in diameter (Fig. 6C, D). In some larger cavities in the wall rocks, the solid bitumen and calcite form clusters on which sulfides precipitated. This structure was likely produced by precipitation of sulfides next to the wall rocks, followed by calcite and solid bitumen in the interiors of the vugs (Fig. 6D).

The microstructural characterization of the bitumen revealed oil droplets and wormlike features suggestive of flow (Fig. 7A). The bitumen is intergrown closely with calcite, galena, sphalerite, and pyrite (Fig. 7B). A symmetrical structure with bitumen and calcite in the center and galena and sphalerite on both sides was observed (Fig. 7C). Finally, occurrences of gypsum crisscrossed by bitumen and pyrite grains in the interstices between celestite crystals were observed locally, and probably represent remnants of the dissolution of larger gypsum crystals (Fig. 7D).

Organic matter in the Triassic sequences

The Lanping basin was filled with a series of marine sequences with abundant organic matter during the late Triassic. From the Jurassic onward, however, the basin underwent organic-poor continental clastic deposition (Third Geological Team, 1984). The Triassic Maichujing and Sanhedong Formations have the highest content of organic matter in the region. The Maichujing Formation was deposited in a marine-terrigenous transitional environment and is composed mainly of carbonaceous mudstone interbedded with silty shale, with abundant banded or netlike organic matter (Fig. 8A, B). The Sanhedong Formation is composed of marine carbonate rocks. In the Jinding ore district, solid bitumen is present on the surfaces of and fractures in carbonate rocks of the Sanhedong Formation (Fig. 8C, D). The microstructural nature of bitumen in the Sanhedong Formation is characterized by strip or oil droplike features indicative of flow (Fig. 8E). Pyrite in bitumen veins is present in the form of aggregates of framboidal pyrite with hexagonal or pseudohexagonal symmetry (Fig. 8F). Sphalerite and galena, however, are absent, which suggests that solid bitumen in the Sanhedong Formation was not affected by the ore-forming fluid and that Fe in the framboidal pyrite was most likely sourced from the sediments.

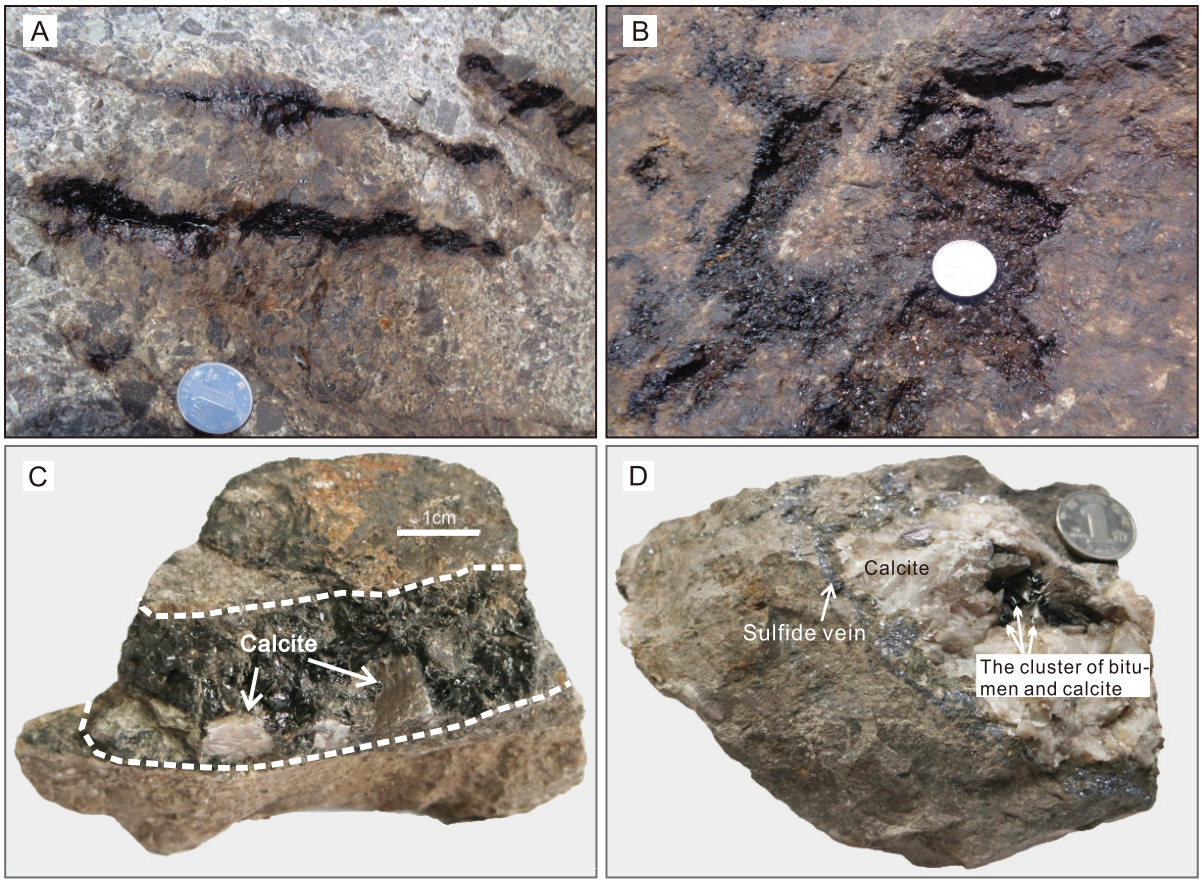

Fig. 6. Various types of organic matter in the Jinding ore district. A. Crude oil in cavities and fissures of wall rock. B. Petroleum accumulated in interstices in the wall rocks. Small calcite crystals on the inner wall of the cavities. C. Vein or tabular-like solid bitumen obviously affected by thermal alteration together with large calcite crystals. D. Clusters of solid bitumen and calcite in the center that are surrounded by sulfides.

Extracts and bulk composition of bitumen

The bulk compositions of the extracts are listed in Table 1. The bituminous ore samples show wide compositional variation of the extracts. Thus, the bitumen content of the ores ranges from 0.0594 to 0.3171 wt %, that of the wall-rock samples to the ores ranges from 0.0150 to 0.0863 wt %, and that of the Sanhedong Formation ranges from 0.0849 to 0.3041 wt %. The organic matter content of the Maichujing Formation ranges from 0.0275 to 0.1764 wt % and that of the Sanhedong Formation ranges from 0.0092 to 0.0370 wt %; the organic matter content of the two samples taken from outside the ore district is within the latter range. The large variation in extractability is attributed mainly to the different organic matter contents of the samples. The contents of saturated hydrocarbons and aromatic hydrocarbons are in the range of 23.91 to 72.91 and 9.82 to 51.69%, respectively, in all analyzed samples (Table 1). The contents of asphaltene and resins are in the ranges of 3.41 to 37.50 and 5.56 to 41.46% and average 10.83 and 15.78%, respectively. The ratio of saturated hydrocarbons to aromatic hydrocarbons ranges from 0.71 to 6.13.

Molecular composition

The carbon number distribution of the *n*-alkane molecules is nC_{11}–nC_{33} for the extracts from the ore samples and nC_{11}–nC_{31} for bitumen from the Sanhedong Formation. With the exception of a sample from the Sanhedong Formation that has two peaks, the bitumen samples all show a single peak with a maximum between nC_{12} and nC_{21}. No significant odd or even carbon number predominance (OEP) of the *n*-alkanes pattern was observed in these bitumen samples (the OEP is close to 1). The carbon preference index (CPI) ranges from 0.72 to 1.05 for bitumen from the ores and from 0.94 to 1.67 for bitumen from the Sanhedong Formation. The ratios of $\Sigma C_{21}^{-}/\Sigma C_{22}^{+}$ and $(C_{21} + C_{22})/(C_{28} + C_{29})$ range from 4.88 to 9.29 and 7.47 to 26.65 for ore bitumen samples and from 3.62 to 7.66 and 9.79 to 15.97 for bitumen samples from the Sanhedong Formation, respectively (Table 2).

The *n*-alkanes in extracts of wall rock and the Upper Triassic samples range from nC_{11} to nC_{33} (Table 2; Fig. 9A, B). Most of the bitumen samples display a single dominant peak with a maximum between nC_{12} and nC_{22}; a few samples show two peaks. The values of OEP and CPI range from 0.72 to 1.12 and 0.74 to 1.02 for samples from wall rock, from 0.99 to 1.34 and 1.03 to 1.64 for samples from the Upper Triassic Maichujing Formation, and from 1.06 to 1.53 and 0.97–1.39 for samples from the Upper Triassic Sanhedong Formation, respectively. The ratios of $\Sigma C_{21}^{-}/\Sigma C_{22}^{+}$ and $(C_{21} + C_{22})/(C_{28} + C_{29})$ range from 3.54 to 7.10 and 13.62 to 24.82 for wall-rock samples, from 1.75 to 5.19 and 8.15 to 13.52 for samples from the Maichujing Formation, and from 0.77 to 3.14 and 5.52

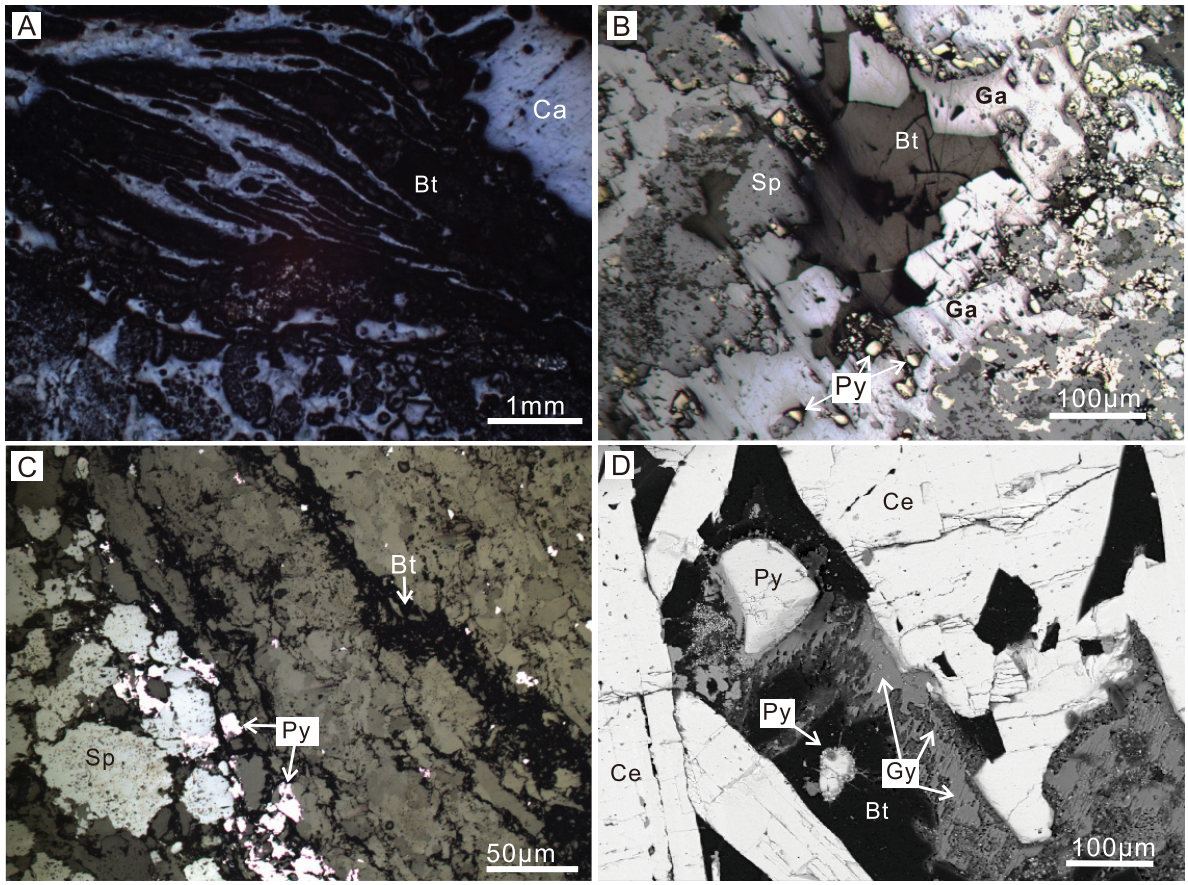

Fig. 7. Microstructural characteristics of organic matter in the ores. A. The microstructural features of bitumen show oil droplets and wormlike and banded features with apparent flow textures. B. Solid bitumen intergrown with galena, sphalerite, and pyrite. C. Sulfides extending along the direction of residual solid bitumen and calcite, with a symmetrical structure from the center to the margins manifested as bitumen, calcite, galena and sphalerite. D. Irregular structure of gypsum with bitumen and pyrite grains in the interspace of celestite, which may represent a relic dissolution structure of gypsum. Abbreviations: Bt = bitumen, Ca = calcite, Ce = celestite, Ga = galena, Gy = gypsum, Py = pyrite, Sp = sphalerite.

to 10.26 for samples from the Sanhedong Formation, respectively (Table 2).

Pristane (Pr) and phytane (Ph) are in lower abundance than the adjacent *n*-alkanes (Fig. 9A, B). They have average Pr/nC_{17} and Ph/nC_{18} values of 0.40 and 0.47 for bitumen samples from ores, 0.41 and 0.69 for bitumen samples from the Sanhedong Formation, 0.37 and 0.35 for wall-rock samples, 0.43 and 0.63 for samples from the Maichujing Formation, and 0.46 and 1.03 for samples from the Sanhedong Formation, respectively (Table 2).

Representative m/z 191 and 217 chromatograms of the saturated fraction are shown in Figure 9. Organic matter extracted from solid bitumen in ores and the Sanhedong Formation and that from the Maichujing and Sanhedong Formation source rocks show very similar distributions of 191 and 217 traces. The C_{19}-C_{25} tricyclic terpanes, C_{24} tetracyclic terpane, hopanes, and gammacerane are abundant in the extracts from the ore, wall rock, and Triassic strata samples, although the relative abundances are different (Fig. 9C, D). The bitumen samples from the ores and the Sanhedong Formation are characterized by similar terpane and sterane distributions, indicating that they originated from similar source rocks. Tricyclic terpanes (TT) with carbon numbers up to C_{29} were detected in all samples, with dominant C_{23} and low C_{19} and C_{22} homologues in most samples.

The relative concentration of homohopanes decreases with increasing carbon number. The relative abundance of C_{29} hopane ($C_{29}H$) in the bitumen samples is lower than that of $C_{30}H$, and the C_{29}/C_{30} hopane ratios range mostly from 0.52 to 0.74 for bitumen in ores, from 0.49 to 0.88 for bitumen samples in the Sanhedong Formation, from 0.56 to 0.67 for wall-rock samples, from 0.51 to 0.59 for samples from the Maichujing Formation, and from 0.66 to 0.97 for samples from the Sanhedong Formation (Table 3). The hopane series were present from C_{27} to C_{35}. Extended hopanes are influenced by the oxidation state of the depositional environment (Waples and Machihara, 1991; Peters and Moldowan, 1993). The similar distributions of the homohopanes in the bitumen of the different types of samples suggests a similar type of source rock, where the homohopanes probably originated from bacteriohopanetetrol and other polyfunctional C_{35} hopanoids common in prokaryotic microorganisms (Peters et al., 2005).

Abundant C_{21} and C_{22} steranes were detected in the sample extracts from the solid bitumen and Triassic strata. The "V" shape in the distribution of C_{27}-C_{29} regular steranes is shown

Table 1. Basic Geochemical Data Showing the Amounts of Solvent Extracts and Proportion of Saturated Hydrocarbon, Aromatic Hydrocarbon, Asphaltene, and Resin in the Extracts for the Solid Bitumens from the Ores and Sanhedong Formation and the Rock Samples from Wall-Rock and Triassic Strata

No.	Sample no.	Samples	Extracts	Sat	Aro	Res	Asp	Res + Asp	Sat/Aro
1	16JD-02	Bt in ore	0.317	45.68	16.64	7.33	30.35	37.68	2.75
2	16JD-05	Bt in ore	0.059	63.42	19.21	10.27	7.14	17.41	3.30
3	16JD-11	Bt in ore	0.097	40.14	43.26	11.50	5.10	16.60	0.93
4	16JDPMP-07	Bt in ore	0.244	58.74	14.25	17.29	9.73	27.02	4.12
5	16PMPJ-02	Bt in ore	0.163	42.44	12.16	7.89	37.50	45.39	3.49
6	16PMPJ-03	Bt in ore	0.281	54.83	19.27	12.48	13.42	25.90	2.85
7	JDD-08	Bt in SHD	0.139	57.20	13.83	18.64	10.34	28.98	4.14
8	JDD-09	Bt in SHD	0.218	52.20	41.83	32.65	15.42	48.07	1.25
9	JDD-10	Bt in SHD	0.121	49.56	28.94	16.23	5.27	21.50	1.71
10	JDD-11	Bt in SHD	0.085	72.91	16.68	6.83	3.57	10.40	4.37
11	JDD-12	Bt in SHD	0.304	36.73	51.69	6.84	4.74	11.58	0.71
12	16JDPMP-02	OM in WR	0.086	50.59	37.09	5.56	6.77	12.33	1.36
13	16JDPMP-03	OM in WR	0.023	63.67	13.54	15.69	7.10	22.79	4.70
14	16PMPJ-04	OM in WR	0.078	56.15	22.32	14.21	7.32	21.53	2.52
15	16PMPJ-07	OM in WR	0.015	60.14	9.82	13.01	17.04	30.05	6.13
16	JDD-04	OM in MCJ	0.038	44.63	37.29	13.57	4.53	18.10	1.20
17	JDD-05	OM in MCJ	0.028	65.83	23.42	6.79	3.96	10.75	2.81
18	JDD-06	OM in MCJ	0.168	63.57	24.44	7.61	4.38	11.99	2.60
19	JDD-07	OM in MCJ	0.176	46.85	37.08	9.18	6.89	16.07	1.26
20	JDD-13	OM in SHD	0.009	33.57	18.84	35.37	12.26	47.63	1.78
21	JDD-14	OM in SHD	0.037	35.68	22.79	32.93	8.62	41.55	1.57
22	GPD	OM in SHD*	0.011	52.98	23.92	19.69	3.41	23.10	2.21
23	GPD	OM in SHD*	0.031	23.91	10.51	41.46	24.12	65.58	2.27

Abbreviations: Aro = aromatics hydrocarbons, Asp = asphaltenes, Bt = bitumen, MCJ = samples from the Maichujing Formation, OM = organic matter, Res = resins, Sat = saturated hydrocarbons, SHD = samples from the Sanhedong Formation, SHD* = samples from the Sanhedong Formation outside the ore district, WR = wall-rock samples

(Fig. 9E, F). The C_{29} sterols can have both vascular plant and algal sources (e.g., green microalgae) (Volkman et al., 1994, 1998; Rontani and Volkman, 2003), although they are often attributed to a terrestrial origin (Huang and Meinschein, 1979; Volkman et al., 1999). Here, the high percentages of C_{29} steranes detected from the bitumen samples are more likely attributable to algae such as benthic brown algae or macro algae, acritarchs, cryptospores, and arthropods rather than a

Table 2. Basic Molecular Parameters for Saturated Hydrocarbon in Bitumen Samples from the Ores and Sanhedong Formation and the Rock Samples from Wall-Rock and Triassic Strata

No.	Sample no.	Samples	Peak type	CND	P_{max}	CPI	OEP	A1	A2	Pr/Ph	Ph/nC_{17}	Ph/nC_{18}
1	16JD-02	Bt in ore	S-P	C_{13}-C_{29}	C_{21}	1.05	1.03	9.29	26.65	0.35	0.24	0.29
2	16JD-05	Bt in ore	S-P	C_{11}-C_{30}	C_{16}	0.93	1.05	7.38	17.17	0.53	0.31	0.58
3	16JD-11	Bt in ore	S-P	C_{12}-C_{30}	C_{20}	0.88	0.93	6.27	7.47	0.69	0.38	0.66
4	16JDPMP-07	Bt in ore	S-P	C_{11}-C_{28}	C_{12}	0.92	1.09	4.88	10.72	0.59	0.44	0.38
5	16PMPJ-02	Bt in ore	S-P	C_{11}-C_{33}	C_{15}	0.72	0.87	9.12	20.26	0.80	0.74	0.57
6	16PMPJ-03	Bt in ore	S-P	C_{12}-C_{30}	C_{17}	0.91	1.01	7.68	14.31	0.58	0.31	0.31
11	JDD-08	Bt in SHD	S-P	C_{14}-C_{28}	C_{17}	0.94	0.97	4.51	12.71	0.52	0.49	0.95
12	JDD-09	Bt in SHD	S-P	C_{14}-C_{28}	C_{17}	1.38	1.29	3.62	15.97	0.62	0.23	0.52
13	JDD-10	Bt in SHD	S-P	C_{15}-C_{29}	C_{20}	0.97	1.02	7.66	15.84	0.93	0.58	0.93
14	JDD-11	Bt in SHD	S-P	C_{11}-C_{33}	C_{21}	1.45	1.47	5.36	9.79	0.41	0.35	0.55
15	JDD-12	Bt in SHD	T-P	C_{12}-C_{29}	C_{17}, C_{27}	1.67	1.13	4.86	10.47	0.23	0.39	0.52
7	16JDPMP-02	OM in WR	S-P	C_{11}-C_{30}	C_{15}	0.92	1.12	4.29	13.62	0.86	0.47	0.41
8	16JDPMP-03	OM in WR	T-P	C_{14}-C_{31}	C_{18}, C_{31}	0.74	0.87	7.10	22.40	0.47	0.42	0.34
9	16PMPJ-04	OM in WR	T-P	C_{11}-C_{29}	C_{12}, C_{29}	0.91	0.72	3.54	19.75	0.88	0.24	0.25
10	16PMPJ-07	OM in WR	S-P	C_{11}-C_{29}	C_{12}	1.02	1.00	7.06	24.82	0.93	0.34	0.39
16	JDD-04	OM in MCJ	S-P	C_{11}-C_{33}	C_{20}	1.03	1.03	2.17	10.28	0.74	0.19	0.67
17	JDD-05	OM in MCJ	S-P	C_{12}-C_{30}	C_{21}	1.21	1.34	1.75	12.73	0.65	0.48	0.61
18	JDD-06	OM in MCJ	S-P	C_{11}-C_{30}	C_{14}	1.25	0.99	5.19	13.52	2.75	0.54	0.72
19	JDD-07	OM in MCJ	T-P	C_{14}-C_{29}	C_{22}, C_{29}	1.64	1.08	4.24	8.15	0.95	0.49	0.53
20	JDD-13	OM in SHD	S-P	C_{13}-C_{30}	C_{20}	0.97	1.07	3.14	9.47	0.38	0.35	1.26
21	JDD-14	OM in SHD	S-P	C_{11}-C_{31}	C_{21}	0.99	1.53	2.79	10.26	0.47	0.49	1.47
22	GPD-02	OM in SHD*	T-P	C_{15}-C_{31}	C_{20}, C_{31}	1.24	1.06	0.77	5.52	0.83	0.56	0.66
23	GPD-03	OM in SHD*	S-P	C_{17}-C_{30}	C_{19}	1.39	1.31	2.57	7.76	0.41	0.42	0.74

Abbreviations: A1= C21-/ C22+, A2 = (C21+C22)/(C28+C29), Bt = bitumen, CND = carbon number distribution, CPI = carbon preference index, MCJ = samples from the Maichujing Formation, OEP = odd or even carbon number predominance, OM = organic matter, Ph = phytane, Pmax = maximum peak, Pr = pristane, S-P = single-peak, SHD = samples from the Sanhedong Formation, SHD* = samples from the Sanhedong Formation outside the ore district, T-P= two peaks, WR = wall-rock samples

terrestrial origin (Volkman et al., 1998; Kodner et al., 2008; Grosjean et al., 2009; Cai et al., 2017). The C_{29} $\alpha\alpha\alpha$ sterane 20R/(20R + 20S) and C_{29} sterane $\beta\beta/(\beta\beta + \alpha\alpha)$ ratios are 0.35–0.72 and 0.54–0.71 for bitumen from the ores and 0.45–0.53 and 0.39–0.54 for bitumen from the Sanhedong Formation. The corresponding ratios for organic matter are 0.42–0.58 and 0.44–0.58 from the wall rocks, 0.37–0.41 and 0.40–0.45 from the Maichujing Formation, 0.35–0.39 and 0.38–0.41 from the Sanhedong Formation, and 0.22–0.38 and 0.31–0.37 in samples of the Sanhedong Formation from outside the ore district (Table 3).

Among the polycyclic aromatic hydrocarbons, the commonly used aromatic compounds in the analysis of source rock, thermal maturity, and the sedimentary environment are phenanthrene (P), methylphenanthrenes (MP), and dibenzothiophene. These hydrocarbons were also detected as shown in the chromatograms of m/z 192 and 198 (Fig. 10).

Sulfur isotopes

The solid bitumen associated with ores in the Jinding deposit yielded two groups of $\delta^{34}S$ values ranging from –24.50 to –16.27‰ and from –7.38 to –4.61‰, respectively. The for-

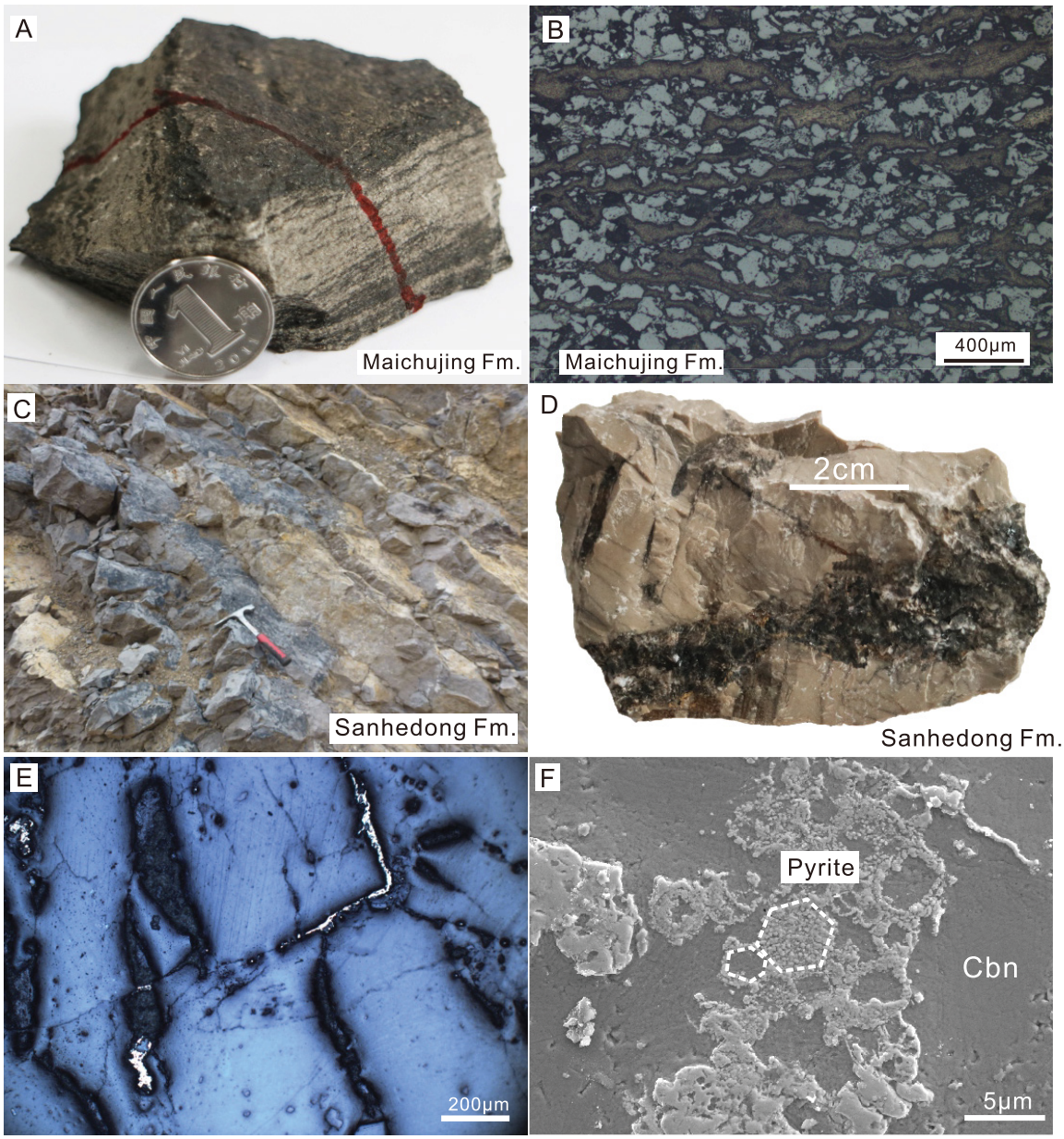

Fig. 8. Different types of organic matter and their microstructural characterization in Triassic strata. A. The carbonaceous mudstone in the Maichujing Formation. B. The banded and net-like organic matter in the Maichujing Formation. C and D. Bitumen on the surface and fractures of carbonate rocks in the Sanhedong Formation. E. Bitumen in the Sanhedong Formation displaying a strip or oil droplike appearance and flow feature together with small pyrite grains at the corner of the bitumen vein. F. Aggregates of framboidal pyrite with hexagonal or pseudohexagonal symmetry or in other forms. Abbreviations: Cal = calcite, Cbn = carbonate rocks.

Table 3. Steranes, Hopanes, and Aromatic Hydrocarbon Parameters of the Bitumen Samples in the Ores and Sanhedong Formation and the Rock Samples in Wall-Rock and Triassic Strata

No.	Sample no.	Samples	$C_{19}TT/C_{23}TT$	$C_{20}TT/C_{21}TT$	$C_{22}TT/C_{21}TT$	$C_{23}TT/C_{21}TT$	$C_{24}TT/C_{23}TT$	$C_{26}TT/C_{25}TT$	$C_{19+20}TT/\Sigma TT$
1	16JD-02	Bt in ore	0.14	0.54	0.39	1.67	0.59	0.48	0.09
2	16JD-05	Bt in ore	0.11	0.63	0.52	1.34	0.55	0.49	0.13
3	16JD-11	Bt in ore	0.49	1.07	0.46	3.72	0.45	0.38	0.33
4	16JDPMP-07	Bt in ore	0.15	0.68	0.26	1.34	0.57	0.51	0.13
5	16PMPJ-02	Bt in ore	0.21	1.28	0.43	0.89	0.63	0.77	0.23
6	16PMPJ-03	Bt in ore	0.07	0.26	0.69	1.32	0.48	0.39	0.05
7	JDD-08	Bt in SHD	0.33	0.87	1.04	2.93	0.31	0.45	0.23
8	JDD-09	Bt in SHD	0.12	0.57	0.58	1.47	0.51	0.39	0.12
9	JDD-10	Bt in SHD	0.07	0.52	0.49	1.24	0.34	0.71	0.12
10	JDD-11	Bt in SHD	0.17	0.68	0.41	1.36	0.53	0.37	0.18
11	JDD-12	Bt in SHD	0.08	0.54	0.72	1.76	0.48	0.46	0.07
12	16JDPMP-02	OM in WR	0.37	1.08	0.31	1.73	0.46	0.31	0.32
13	16JDPMP-03	OM in WR	0.11	0.67	0.39	2.05	0.50	0.44	0.10
14	16PMPJ-04	OM in WR	0.06	0.51	0.43	1.28	0.55	0.87	0.11
15	16PMPJ-07	OM in WR	0.07	0.56	0.47	1.73	0.51	0.37	0.06
16	JDD-04	OM in MCJ	0.13	0.57	0.23	0.92	0.51	0.66	0.17
17	JDD-05	OM in MCJ	0.07	0.87	0.22	1.43	0.44	0.38	0.14
18	JDD-06	OM in MCJ	0.10	0.64	0.38	1.86	0.62	0.35	0.07
19	JDD-07	OM in MCJ	0.21	0.36	0.40	1.15	0.47	0.46	0.19
20	JDD-13	OM in SHD	0.18	0.46	0.47	2.25	0.43	0.28	0.18
21	JDD-14	OM in SHD	0.23	0.68	0.55	1.16	0.45	0.32	0.15
22	GPD-02	OM in SHD*	0.31	0.54	0.67	3.39	0.54	0.41	0.29
23	GPD-03	OM in SHD*	0.07	0.72	1.09	1.47	0.23	0.39	0.09

Abbreviations/notes: Bt = bitumen, MCJ = samples from the Maichujing Formation, OM = organic matter, SHD = samples from the Sanhedong Formation, SHD = samples from the Sanhedong Formation outside the ore district, WR = wall-rock samples; MDR = 4-MDBT/1-MDBT (Radke et al., 1986), MPR = 2-MP/1-MP (Radke et al., 1982); MPI1 = 1.5*(2-MP+3-MP)/(P+1-MP+9-MP) (Radke et al., 1982), TT = tricyclic terpanes, T2 = C29 $\alpha\alpha\alpha$ sterane 20R/(20R+20S), %Rc = 2.3–0.6MPI1 (Rc>1.35%) for samples no. 1–15, and %Rc = 0.4 + 0.6MPI1 (Rc<1.35%) for samples no. 16–23 (Radke and Welte, 1983), %Rb= (Rc-0.4)/0.618 (Jacob, 1989); the calculated Rb values with * symbol are consistent with the measured reflectance of bitumen (2.51 and 1.83 for 16JD-11 and JDD-09, respectively), - = no data

mer group shows large overlap with the $\delta^{34}S$ values of solid bitumen from the Triassic Sanhedong Formation, which has $\delta^{34}S$ values of –27.62 to –17.38‰ (Table 4; Fig. 11).

The previously published sulfur isotope values for sulfide minerals from the Jinding deposit show a large variation in $\delta^{34}S$ values from –30.43 to –1.33‰ with an average of –14.52‰. The $\delta^{34}S$ values of sphalerite, pyrite, and galena are from –23.35 to –1.71‰ (avg, –13.67‰), –23.46 to –3.36‰ (avg, –15.22‰), and –30.43 to –1.33‰ (avg, –14.10‰), respectively (Fig. 11; Ye et al., 1992; Zhou and Zhou; 1992; Chen, 2015). Most of the $\delta^{34}S$ values for these sulfide minerals are distributed into two groups, –30 to –10‰ and –8 to 0‰, which correspond to the early and late stages of mineralization, respectively (Fig. 11; Tang et al., 2014). The $\delta^{34}S$ values of evaporite sulfates that are widely distributed in the Lanping basin, especially in the Jinding district, range from 7.3 to 25.2‰, with the majority of values between 7.3 and 16.3‰ (Qin and Zhu, 1991; Hu et al., 2013; Wang, 2013).

Discussion

Thermal maturity of the bitumen

Analyses of the solid bitumen samples from the ores and the Triassic Sanhedong Formation show that the values of the CPI, a thermal maturity indicator, ranges from 0.72 to 1.67 and that the OEP values are from 0.87 to 1.47. These values, which are very close to 1.0, indicate a high degree of maturity (Bray and Evans, 1961; Clark and Blumer, 1967; Dembicki et al., 1976). The lower CPI and OEP values for bitumen from the ores and their generally higher values of $\Sigma n\text{-}C_{21}^{-}/\Sigma n\text{-}C_{22}^{+}$ and $(C_{21} + C_{22})/(C_{28} + C_{29})$, however, indicate that this bitumen is slightly more mature than the bitumen from the Sanhedong Formation (Table 2).

The methyl phenanthrene index (MPI1 = 1.5*(2-MP + 3-MP)/(P + 1-MP+ 9-MP)), which is based on phenanthrene and the four methyl phenanthrenes (3-, 2-, 9-, and 1-) (Fig. 10A, B), is one of the most widely used maturity parameters (Radke et al., 1982, 1986; Radke and Welte, 1983; Radke, 1988) and is often applied in estimating the equivalent vitrinite reflectance value (Rc) of crude oils and source rocks (Rc = 2.3–0.6MPI1 [Rc >1.35%], Rc = 0.4+0.6MPI1 [Rc ≤1.35%]; Radke and Welte, 1983). The calculated MPI1 and Rc values were 0.31–1.01 and 1.69–2.11% for bitumen from the ores and 1.07–1.21% and 1.57–1.66% for bitumen from the Sanhedong Formation, respectively (Table 3). The corresponding calculated reflectance of the bitumen (Rb) is 2.09–2.77 with an average of 2.49 and 1.90–2.04 with an average of 1.96, respectively (%Rb = (Rc-0.4)/0.618; Jacob, 1989). The vitrinite reflectance of a bitumen sample from ore and another from the Sanhedong Formation (16JD-11, JDD-09) were found to be 2.51 and 1.83, respectively. These values are consistent with the calculated reflectance values of bitumen samples from the MPI1, showing that the bitumen in ores reached higher maturity than in the Sanhedong Formation. This conclusion is supported by the higher ratios of 4- and 1-methyl diphenylthiophene (MDR) and 2- and 1-methyl phenanthrenes (MPR), respectively, in bitumen from the ores than in bitumen from the Sanhedong Formation (Table 3). The reason for the latter interpretation is that 4-MDR and 2-MPR have

Table 3. (*Cont.*)

No.	$C_{29}H/C_{30}H$	$C_{35}S/C_{34}S$	$C_{31}R/C_{30}H$	$G/C_{30}H$	$G/C_{31}S$	T1	T2	MDR	MPR	MPI1	Rc (%)	Rb (%)
1	0.57	0.82	0.34	0.07	0.68	0.59	0.72	9.73	2.77	0.31	2.11	2.77
2	0.63	0.62	0.48	0.19	1.67	0.69	0.63	6.24	2.19	0.43	2.04	2.66
3	0.52	0.59	0.39	0.19	0.91	0.54	0.35	3.63	1.76	0.87	1.78	2.23*
4	0.53	0.46	0.36	0.29	1.18	0.57	0.56	5.46	2.14	0.52	1.99	2.57
5	0.74	0.98	0.25	0.15	1.24	0.67	0.63	7.89	2.22	1.01	1.69	2.09
6	0.63	0.86	0.34	0.18	1.31	0.71	0.51	5.14	2.26	0.46	2.02	2.63
7	0.72	0.87	0.46	0.23	1.47	0.54	0.47	5.13	1.97	1.07	1.66	1.90
8	0.88	0.97	0.37	0.11	0.84	0.39	0.47	4.05	1.89	1.16	1.60	1.95*
9	0.49	0.83	0.31	0.19	1.73	0.52	0.53	6.23	2.08	1.21	1.57	2.04
10	0.57	0.51	0.43	0.26	0.78	0.43	0.49	4.93	2.11	1.19	1.59	1.92
11	0.58	0.75	0.39	0.15	1.33	0.47	0.45	4.87	1.92	1.09	1.65	2.02
12	0.60	0.62	0.48	0.26	1.30	0.58	0.56	5.93	2.54	1.36	1.48	-
13	0.57	0.79	0.35	0.14	1.22	0.55	0.58	6.72	2.01	0.50	2.00	-
14	0.56	0.68	0.18	0.18	1.60	0.50	0.54	5.47	2.29	1.14	1.62	-
15	0.67	0.87	0.31	0.09	0.75	0.44	0.42	3.63	2.06	0.53	1.98	-
16	0.57	0.55	0.28	0.25	1.57	0.43	0.39	4.47	1.86	0.99	0.99	-
17	0.55	0.72	0.32	0.16	1.14	0.40	0.37	4.52	1.89	0.53	0.72	-
18	0.51	0.61	0.29	0.11	1.87	0.45	0.37	4.31	1.78	0.76	0.85	-
19	0.59	0.39	0.26	0.15	0.88	0.42	0.41	5.61	1.94	1.25	1.15	-
20	0.68	0.77	0.39	0.15	1.17	0.38	0.35	4.08	1.54	0.90	0.94	-
21	0.66	0.93	0.41	0.22	1.65	0.41	0.39	4.37	1.71	0.76	0.86	-
22	0.94	1.19	0.38	0.09	0.46	0.37	0.38	3.79	1.53	1.08	1.05	-
23	0.97	1.09	0.47	0.24	1.66	0.31	0.22	2.74	1.49	0.35	0.61	-

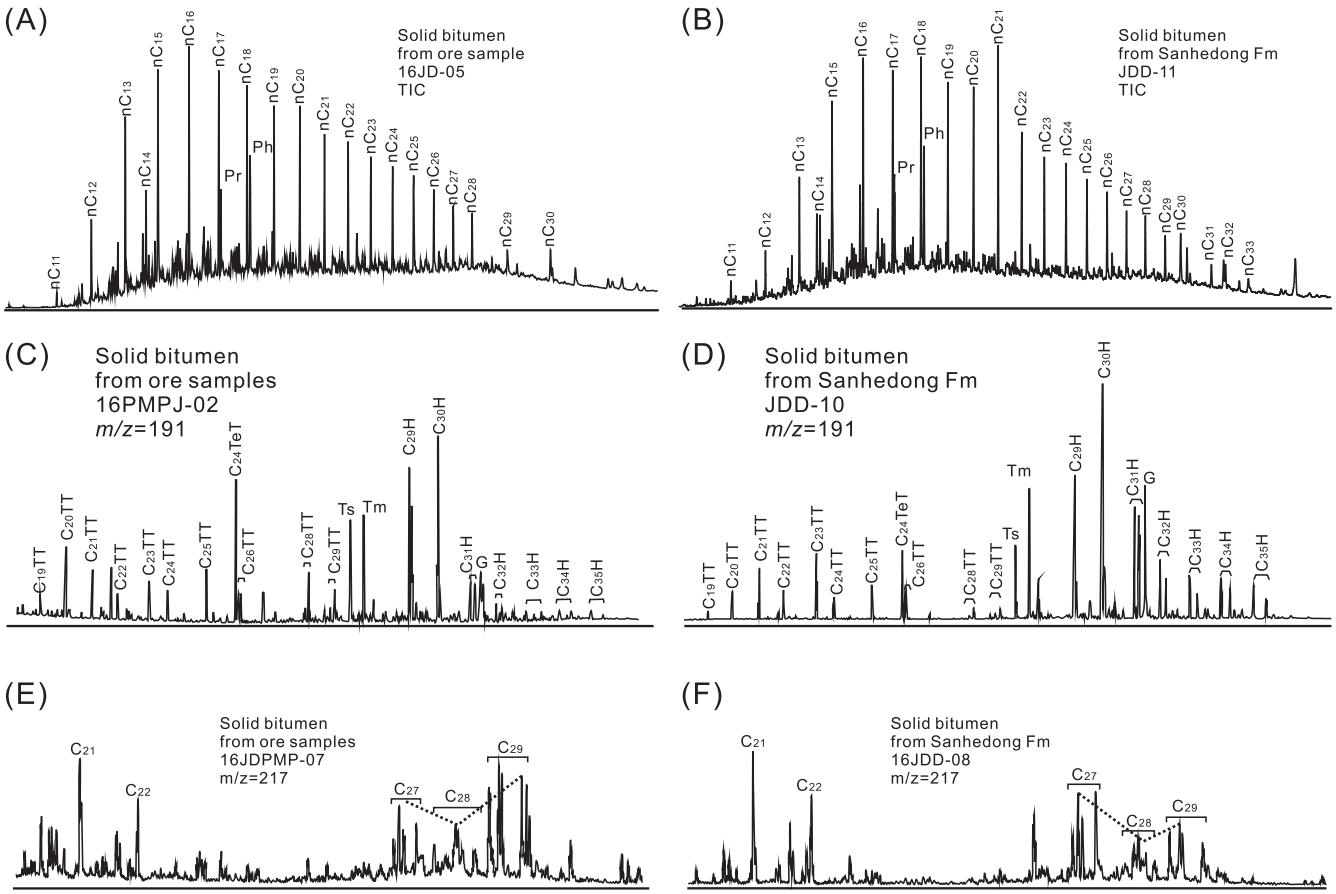

Fig. 9. Representative saturated hydrocarbon fraction gas chromatogram (A and B). *m/z* = 191 (C and D) and *m/z* = 217 (E and F) chromatograms showing *n*-alkanes, terpane, hopane, and sterane distributions for extractable organic matter from the bitumens in ores and the Sanhedong Formation.

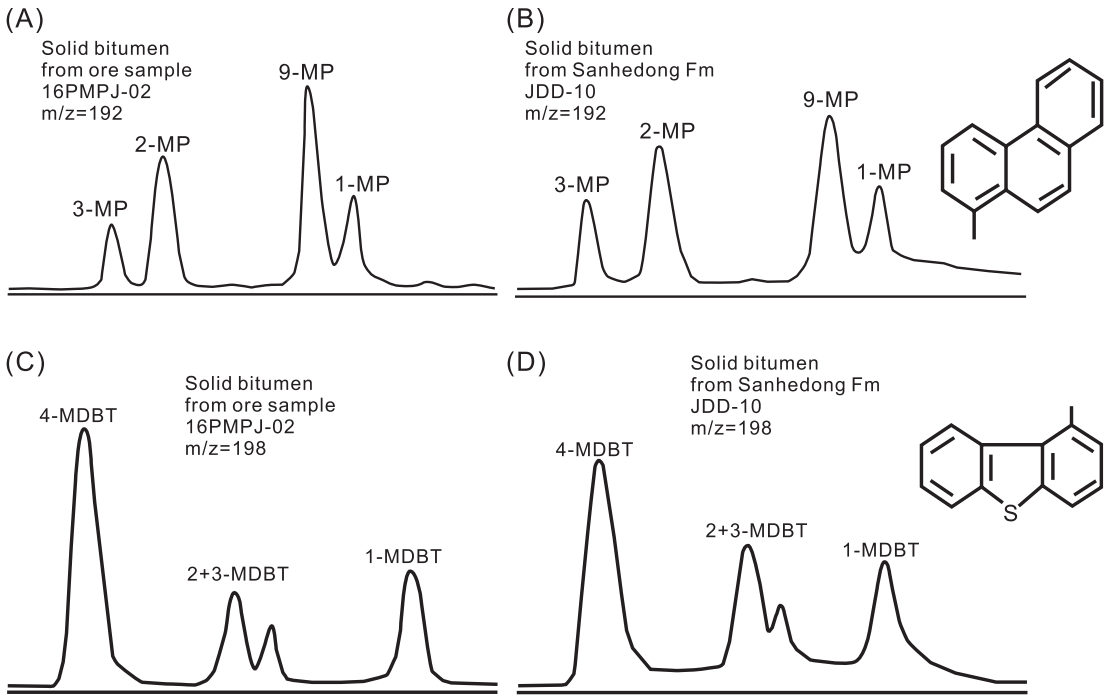

Fig. 10. Chromatograms showing methylphenanthrene (MP, m/z = 192) and dibenzothiophene (DBT, m/z = 198) of bitumen from ores and the Sanhedong Formation.

higher stability than 1-MDR and 1-MPR, respectively (Radke et al., 1982, 1986; Hughes et al., 1995).

Among maturity-related parameters, the sterane ratios C_{29} $\alpha\alpha\alpha$ sterane 20S/(20S + 20R) and C_{29} sterane $\beta\beta/(\beta\beta+\alpha\alpha)$ are widely used in petroleum geochemistry as indicators of thermal maturity to investigate oil or source rock evolution through the "oil window" (Seifert and Moldowan, 1986; Rullkötter and Marzi, 1988; Farrimond et al., 1998). The equilibrium end points of the two ratios are 0.50–0.55 and 0.67–0.71, respectively (Mackenzie and McKenzie, 1983; Seifert and Moldowan, 1986). In this study, the values of C_{29} $\alpha\alpha\alpha$ 20S/(20S + 20R) and C_{29} sterane $\beta\beta/(\beta\beta + \alpha\alpha)$ ranged from 0.35 to 0.72 and 0.54 to 0.71, respectively, for bitumen in the ores and from 0.45 to 0.53 and 0.39 to 0.54, respectively, for bitumen from the Sanhedong Formation (Table 3, Fig. 12), suggesting that the solid bitumen in the ores and the Sanhedong Formation is very mature but has higher maturity in the ores.

The presence of short-chain steranes also indicates the high thermal maturity of the bitumen in the ores and in the Sanhedong Formation. In general, the C_{21} 5α-sterane and C_{22} 5α-sterane are present in oil and source rocks in much lower abundance than the C_{27}-C_{29} steranes. The abnormally

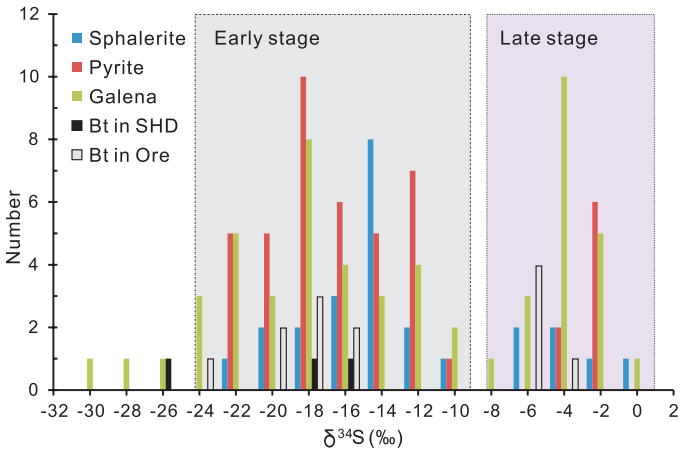

Fig. 11. Histograms showing the distribution of δ^{34}S values of solid bitumen in ores and the Sanhedong Formation and sulfides in the early and late mineralization stages in the Jinding Zn-Pb deposits. Values of δ^{34}S for sulfides reported by Ye et al. (1992), Zhou and Zhou (1992), and Chen (2015). Abbreviations: Bt = bitumen, SHD = Sanhedong Formation.

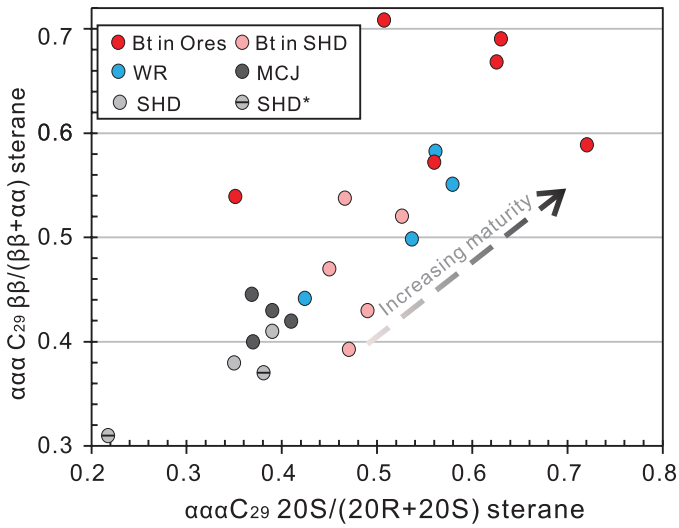

Fig. 12. Cross-plot of biomarker ratios C_{29}-$\beta\beta/(\beta\beta + \alpha\alpha)$ versus C_{29}-20S/(20S + 20R) for bitumen in ores, the Sanhedong Formation (SHD, SHD*), wall rocks, and Triassic strata.

Table 4. $\delta^{34}S$ Values of Solid Bitumens in the Ores and Sanhedong Formation

No.	Sample no.	Samples	$\delta^{34}S$ (‰)
1	16JDD-08	Bt in SHD	–17.38
2	16JDD-09	Bt in SHD	–27.62
3	16JDD-10	Bt in SHD	–19.67
4	16JD-02	Bt in ore	–20.17
5	16JD-11	Bt in ore	–18.37
6	16JDPMP-07	Bt in ore	–17.84
7	16PMPJ-02	Bt in ore	–6.71
8	Bit-1	Bt in ore	–16.27
9	Bit-4	Bt in ore	–6.84
10	Bit-5	Bt in ore	–7.38
11	Bit-6	Bt in ore	–6.1
12	Bit-7	Bt in ore	–4.61
13	Bit-8	Bt in ore	–19.49
14	Bit-9	Bt in ore	–21.66
15	Bit-10	Bt in ore	–24.5
16	Bit-11	Bt in ore	–18.69

Numbers 8–16 data cited from Chen (2015); Abbreviations: Bt = bitumen, SHD = samples from the Sanhedong Formation

high abundance of C_{21} 5α-sterane and C_{22} 5α-sterane is related primarily to high maturity (Wingert and Pomerantz, 1986; Huang et al., 1994) or a moderately hypersaline depositional environment (Requejo et al., 1997; Wang et al., 2010). In this study, the C_{21} 5α-sterane and C_{22} 5α-sterane were present in both bitumen samples at significantly high levels (Fig. 9E, F), which more likely resulted from the higher maturity revealed by other biomarker parameters for these bitumen samples.

The higher thermal maturity of the bitumen in the ores indicates that it was probably generated by a high-temperature process (such as the thermal cracking of oil). The lower maturity of the bitumen in the Sanhedong Formation, however, could suggest that it was the product of a lower-temperature process (e.g., de-asphalting of oil or biodegradation).

The values of CPI and OEP, $\Sigma n\text{-}C_{21}^{-}/\Sigma n\text{-}C_{22}^{+}$, $(C_{21} + C_{22})/(C_{28} + C_{29})$, and the calculated Rc values (Tables 2, 3) show that the organic matter in the wall rocks is of maturity similar to that of the solid bitumen in the ores but is more mature than organic matter in the Sanhedong Formation. This is interpreted to reflect the heat of the ore-forming hydrothermal fluids and the lack of such heat elsewhere in the Sanhedong Formation, which is consistent with the observation that organic matter from the Sanhedong Formation within and outside the ore district has the same thermal maturity. The sterane ratios C_{29} $\alpha\alpha\alpha$ sterane 20S/(20S + 20R) and C_{29} sterane $\beta\beta/(\beta\beta + \alpha\alpha)$ also support the above conclusion (Fig. 8).

The sedimentary environment and potential source rock for the bitumen

The abundant residual organic matter and crude oil that are present on wall-rock surfaces or accumulated in cavities and fissures of the wall rocks (Figs. 6, 7), together with the widespread occurrence of solid bitumen, oil, and gas inclusions (Xue et al., 2007b, 2009; Chi et al., 2017), suggest that there was a paleo-oil reservoir at the site of the Jinding deposit (Jinding dome) before and/or during mineralization (Song et al., 2020). According to this hypothesis, hydrocarbons in the paleoreservoirs were altered to bitumen during mineralization when ore-forming hydrothermal fluid entered the dome.

The ratios Pr/Ph, Pr/nC_{17}, and Ph/nC_{18} are commonly used as biomarker parameters in the analysis of sedimentary environments and in relating oils to their potential sources. Low values of these parameters (<1.0) generally are indicative of an anoxic environment (Didyk et al., 1978; Peters et al., 2005) and are commonly associated with a stratified water column or a hypersaline environment. Most of the values of the above ratios for solid bitumen in the ores and the Sanhedong Formation are <1.0 (in the range of 0.23–1.47, average 0.61; Table 2), indicating that the environment was anoxic. The *n*-alkane distribution, with relatively low values of Pr/Ph, Pr/nC_{17}, and Ph/nC_{18} (Table 2), indicate a strongly anoxic depositional environment with considerable marine organic matter input into the source rocks for this solid bitumen. Moreover, the cross-plot of Pr/nC_{17} versus Ph/nC_{18} indicates that the bitumen likely originated from marine source rocks with an algal input (Fig. 13A).

Peters et al. (2005) used plots of $C_{22}TT/C_{21}TT$ versus $C_{24}TT/C_{23}TT$, $C_{29}H/C_{30}H$ versus $C_{35}S/C_{34}S$, and $C_{26}TT/C_{25}TT$ versus $C_{31}R/C_{30}H$ (TT = tricyclic terpane) for more than 500 worldwide crude oil samples to predict source-rock depositional environments (marine, lacustrine, carbonate, marl, and evaporate). In Figure 13, we present these plots for the data obtained in this study (Table 2) and use them to identify the source-rock environment for the Jinding bitumen. Most of our bitumen samples plot in the fields of marine shale and marl, and few lie in the carbonate field. Thus, these data indicate that the source rocks for the bitumen samples were likely a mixed marine shale and carbonate, which is consistent with the conclusions that can be drawn from a plot of Pr/Ph versus $G/C_{30}H$ (Fig. 14A).

The regional geologic data suggest that the late Triassic strata in the study area are the most likely source rocks for the solid bitumens in the ores and Sanhedong Formation. Indeed, the shale and carbonate rocks in the Upper Triassic Sanhedong and Maichujing Formations show a high hydrocarbon-generating potential and thermal maturity, as revealed by Rc values ranging from 0.61 to 1.15%, and thus are considered to be the main source rock for hydrocarbons in the Lanping basin (Wang and Zhang, 2003; Xue et al., 2009).

The distribution of terpanes, hopanes, and steranes shows that the bitumen in the ores and Sanhedong Formation have a similar source (Fig. 9). In addition, the correlations between the various biomarker parameters, i.e., $C_{22}TT/C_{21}TT$ versus $C_{24}TT/C_{23}TT$, $C_{29}H/C_{30}H$ versus $C_{35}S/C_{34}S$, and $C_{26}TT/C_{25}TT$ versus $C_{31}R/C_{30}H$ (Fig. 13), and numerous parameters derived from these biomarkers support the hypothesis that the bitumen originated from late Triassic source rocks (Fig. 14). Most of the bitumen samples in the current study have low values of $C_{19}TT/C_{23}TT$, C_{19+20} TT/ΣTT, and a $C_{23} > C_{21} > C_{20}TT$ distribution (Fig. 14), similar to those of marine source rocks (Xiao et al., 2019). Moreover, the gammacerane index $G/C_{30}H$ and $G/C_{31}S$ (H = hopane, G = gammacerane, $C_{31}S$ = C_{31}Hopane–22S) is generally thought to be related to the salinity of the depositional environment of the source rocks (Hanson et al., 2000; Holba et al., 2003; Summons et al., 2008; Chen et al., 2016). In this study, most of the bitumen has $G/C_{30}H$ and $G/C_{31}S$ ratios consistent with the organic matter in the Upper Triassic shales and carbonates (Fig. 14D), indicating that the source rock of bitumen in the ores and the Sanhe-

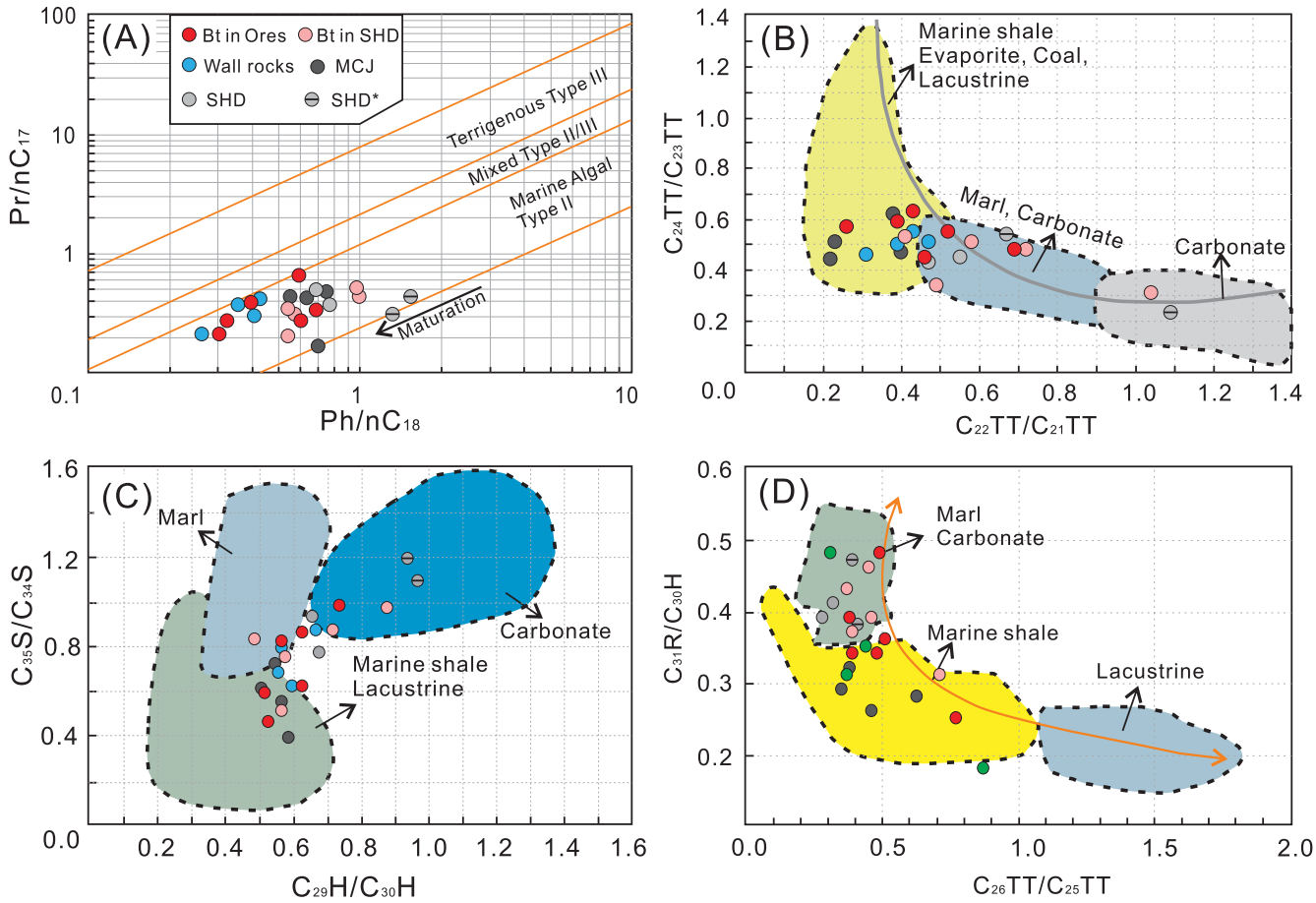

Fig. 13. Binary plots of biomarker ratios in bitumen from ores, the Sanhedong Formation (SHD, SHD*), wall rocks, and Triassic strata (A) pristane (Pr)/nC_{17} versus phytane (Ph)/nC_{18} (after Shanmugam, 1985), (B) $C_{22}TT/C_{21}TT$ versus $C_{24}TT/C_{23}TT$, (C) $C_{29}H/C_{30}H$ versus $C_{35}S/C_{34}S$, and (D) $C_{26}TT/C_{25}TT$ versus $C_{31}R/C_{30}H$.

dong Formation deposited under conditions similar to those of the Upper Triassic shales and carbonates. In summary, the results of this study show that the bitumen and organic matter in the Triassic samples have similar distributions of the biomarkers and their ratios, strongly suggesting that late Triassic rocks were probably the source for the hydrocarbons that occupied the paleo-oil reservoirs represented by the bitumen in the Jinding deposit.

Generation of the H_2S

A large amount of H_2S was required to form the giant Jinding Zn-Pb deposit, although it is unclear how it originated. The sulfur isotope compositions of sulfide minerals in the Jinding deposit vary widely, with $\delta^{34}S$ values ranging from –30 to –10‰ in the early mineralization stage and from –8 to 0‰ during late mineralization (Fig. 11). In this respect, the Jinding deposit is quite different from other Zn-Pb deposits, e.g., MVT deposits, sandstone-hosted deposits (Laisvall deposit), and sedimentary exhalative deposits, which are strongly enriched in ^{34}S (Fig. 15; Huang et al., 2004; Leach et al., 2005; Saintilan et al., 2016). It is also very different from the adjacent Zn-Pb deposits in the Chuan-Dian-Qian metallogenic region of the western part of the South China block (Fig. 15; Huang et al., 2004; Yuan et al., 2014; Zhou et al., 2014).

In cases where organic matter is present, MSR and TSR have been proposed as the two main mechanisms for producing H_2S (Orr, 1977; Machel, 2001; Hoefs, 2004; Basuki et al., 2008). The upper and lower limits of the range of $\delta^{34}S$ values of the sulfide minerals in the early (main) mineralization stage (–30 to –10‰) are roughly 35‰ less than the corresponding limits for the sulfate (gypsum/anhydrite) $\delta^{34}S$ values in the Lanping basin (7.3–25.2‰). This difference is much larger than any reported for natural TSR, which is thought to produce a sulfur isotope fractionation of no more than 20‰ (Machel et al., 1995; Worden and Cai, 2006, King et al., 2014; Cai et al., 2017). It therefore follows that TSR is highly unlikely to have been the main process by which H_2S was produced in this mineralization stage. Much larger fractionation of sulfur isotopes, however, is possible with MSR, up to 71‰ (Goldhaber and Kaplan, 1975; Canfield and Teske, 1996). We therefore propose that the sulfur required to form the main mineralizing stage in the Jinding deposit was derived from MSR. The key questions are where and how the MSR-derived H_2S formed and contributed to mineralization.

An open system and favorable temperature are necessary for MSR (Furusaka, 1961; Orr, 1977; Machel, 1987b, 2001; Wing and Halevy, 2014). The relatively high ore-forming temperature (>100°C) predicted by the fluid-inclusion homogenization temperatures suggests that MSR is unlikely to have

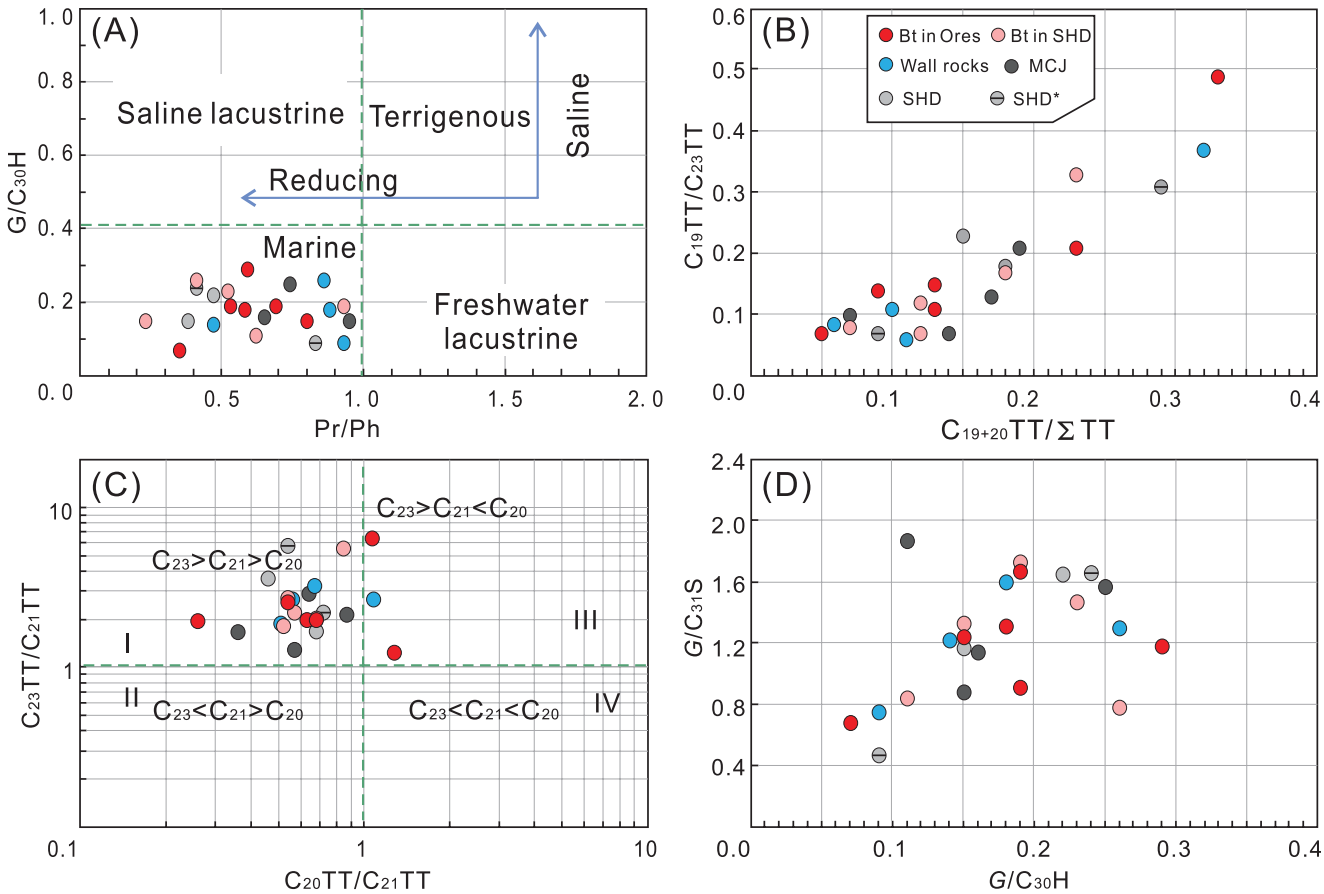

Fig. 14. Correlations between various biomarker parameters reflecting organic matter input and depositional environment. (A) Pr/Ph versus $G/C_{30}H$, (B) $C_{19+20}TT/\Sigma TT$ versus $C_{19}TT/C_{23}TT$, (C) $C_{20}TT/C_{21}TT$ versus $C_{23}TT/C_{21}TT$, and (D) $G/C_{30}H$ versus $G/C_{31}S$. The correlations also show that the bitumen from the ores and Sanhedong Formation (SHD, SHD*) correlated well with the Triassic strata.

occurred at the time of mineralization. Thus, H_2S was generated at a site different from that of mineralization, as was the case for the Zhaolanzhuang reservoirs in the Bohai bay basin where the H_2S is interpreted to have been derived from MSR in the source rock prior to migration. There the fractionation in $\delta^{34}S$ between anhydrite and H_2S is up to 33% (Cai et al., 2005; Worden and Cai, 2006).

The $\delta^{34}S$ values in solid bitumen from the ores (–24.50 to –16.27‰) are similar to those of sulfide minerals in the early mineralization stage and to that of solid bitumen from the Sanhedong Formation ($\delta^{34}S$ = –27.62 to –17.38‰). Studies have shown that H_2S can be incorporated into organic matter by reacting with organic matter to form organosulfur compounds, thereby leading to lower $\delta^{34}S$ values (Sinninghe Damst´e and de Leeuw, 1990). The strongly depleted $\delta^{34}S$ values of solid bitumen from the ores and the Sanhedong Formation therefore can be explained by the incorporation of H_2S. Thus, the similar range of $\delta^{34}S$ values of the mainstage sulfides and solid bitumen in the Jinding deposit might be the result of their having the same origin as solid bitumen in the Sanhedong Formation. Taken in conjunction with the evidence that the solid bitumen in the ores and in the Sanhe-

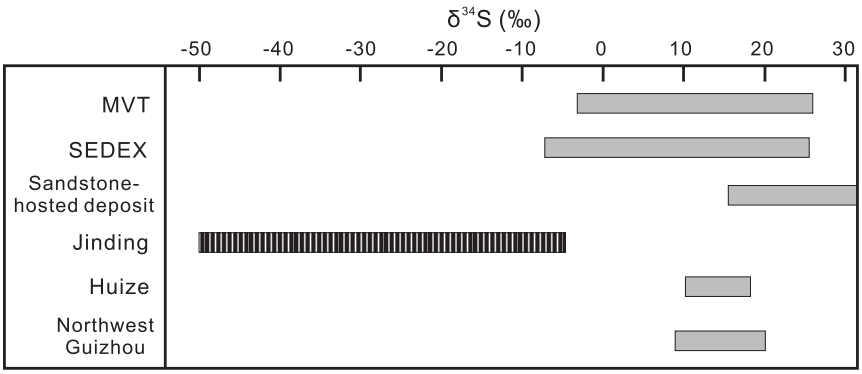

Fig. 15. $\delta^{34}S$ value ranges of sulfides from different types of Zn-Pb deposits and specific deposits in China, including Jinding.

dong Formation had a similar origin, it is reasonable to propose that the MSR occurred in the late Triassic strata prior to or during migration of the hydrocarbons to the Jinding dome to form the paleo-oil reservoir. We propose that this occurred when the Triassic sequences were uplifted as a result of Meso-Cenozoic tectonic activity (Liu et al., 1999; Fu, 2005). The MSR-derived H_2S is therefore interpreted to have coexisted with the hydrocarbons in the paleo-reservoir prior to mineralization. The middle Jurassic Huakaizuo Formation that is rich in argillaceous material and has a low permeability, was likely a good cap rock, as in the case of No. 1 orebody in the Jinding deposit (Third Geological Team, 1984; Xue et al., 2007a).

Conditions would have been ideal for sulfate-reducing microbes to live in the Triassic strata, especially in the Sanhedong Formation. First, the lithological features and biomarker maturity parameters suggest that solid bitumen in the Triassic strata has lower thermal maturity than in the ores (Figs. 6–8, 12), indicating that the bitumen in the Sanhedong Formation likely formed by a low-temperature process that made it possible for sulfate-reducing microbes to survive. Moreover, the occurrence of MSR is supported by the presence of abundant organic matter and syngenetic laminar gypsum in the Sanhedong Formation (Zhang, 2018). The aggregates of framboidal pyrite in the Sanhedong Formation (Fig. 8F) are also good evidence that sulfate-reducing microbes were present; pyrite framboids are thought to be a consequence of sulfate-reducing microbial activity (Schoonen, 2004; Picard et al., 2018).

In conclusion, MSR most likely occurred in the Triassic strata prior to or during migration of hydrocarbons to the Jinding dome together with oil and gas that were sourced from organic matter in the marine Upper Triassic source rocks. Large amounts of MSR-derived H_2S could have been present in the paleoreservoirs in the Jinding dome before mineralization. We propose that this H_2S mixed with hot metalliferous fluids during the early mineralization stage and that the H_2S reacted with the aqueous metal species and precipitated rapidly as fine-grained and disseminated sulfide minerals (sphalerite, galena, and pyrite; Fig. 3E). Also, we propose that the hydrocarbons in the paleoreservoir were altered to solid bitumen due to this interaction with the metalliferous hydrothermal fluids, incorporating MSR-derived H_2S in the process and thereby accounting for the strongly depleted $\delta^{34}S$ values of the bitumen.

The elevated $\delta^{34}S$ values of the sulfide minerals of the late mineralization stage (–8 to 0‰) suggest that the H_2S was likely generated by TSR; the difference in $\delta^{34}S$ values between sulfates (gypsum/anhydrite) and H_2S was generally not more than 20%, which is consistent with TSR (Machel et al., 1995; Cai et al., 2005, 2017; Worden and Cai, 2006, King et al., 2014;). This interpretation is supported by the observation that organic matter was abundant in the paleohydrocarbon reservoir of the Jinding dome and the presence of sulfate minerals. The hydrocarbons were possibly oxidized by sulfate to form the bitumen residues in ores. The TSR-altered solid bitumen could have incorporated large amounts of TSR-derived H_2S, causing the $\delta^{34}S$ values to be significantly higher than those of the solid bitumen not altered by TSR (Kelemen et al., 2008; Cai et al., 2017). This would explain the higher $\delta^{34}S$ value (–7.38 to –4.61‰) of some of the solid bitumen from ores (Table 4, Fig. 11). We also note that as nonaqueous mixtures of hydrocarbons and solid sulfates remain unreactive even at temperatures as high as 180° to 315°C (Toland, 1960), the abundant gypsum and/or anhydrite that are widely distributed in the Jinding area (Fig. 5; Song et al., 2020) might have dissolved to produce sulfate ions. Indeed, this is indicated by the dissolution textures observed in gypsum (Fig. 7D). The high salinity of the ore-forming fluids (Xue et al., 2007a; Zeng, 2007) would also have facilitated the dissolution of sulfate (Blount, 1977; Hanor, 2000). It is noteworthy that experimental and fluid-inclusion data from sour gas fields suggest that the lowest temperature for TSR is about 100° to 140°C (Goldhaber and Orr, 1995; Machel, 1987a; Worden et al., 1995). In the Jinding deposit, the ore-forming temperature (115°–250°C) revealed by fluid-inclusion studies (Xue et al., 2007a; Zeng, 2007) is higher than the lower temperature limit of TSR and thus is favorable for TSR. Moreover, the euhedral dolomite granules in the cavities of solid bitumen (Fig. 16A) suggest that the Mg^{2+} concentration was high in the ore-forming fluid, which would have facilitated TSR (Zhang et al., 2012). Significantly, organic acid, which is a by-product of TSR, is considered to increase the solubility of quartz (Bennett, 1991; Knauss et al., 1997; Machel, 2001; Greenwood et al., 2013). The dissolution of detrital quartz and reprecipitation as cement during mineralization (Fig. 16B) are therefore further evidence of TSR during the late mineralization stage. We therefore conclude that TSR-derived H_2S led to the precipitation of sulfide during the late mineralization.

Zn-Pb mineralization of the Jinding deposit

The Lanping basin underwent a complex evolution from a late Triassic ocean basin to a Jurassic-Cretaceous continental depression basin and to a Cenozoic pull-apart continental basin (Xue et al., 2002, 2007a). During the late Triassic, hundreds of thick, organic-rich marine sequences deposited and subsequently became the potential source rocks for the paleo-hydrocarbon reservoir in the Jinding dome (Xue et al., 2009). The organic matter in these strata likely reached thermal maturation by compaction and probably also by heat from the strong Himalayan magmatism within the basin (Yin et al., 1990; Xue et al., 2002).

The tectonic activity in the early Cenozoic resulted in a major unconformity between the Cretaceous and Paleogene formations and the uplifting, folding, and thrusting of the Meso-Cenozoic sequences (Fig. 2; Xue et al., 2002). The paleoreservoirs likely formed during this period, and hydrocarbons that likely derived from the Triassic marine carbonates migrated into these reservoirs, including that of the Jinding dome. The Re-Os dating of solid bitumen suggests that the paleohydrocarbon reservoirs probably formed at 68 ± 5 Ma (Gao et al., 2012). The H_2S in the Jinding reservoir would have been derived from MSR that occurred prior to or during the migration of hydrocarbons to the Jinding dome (Song et al., 2020) when the Triassic sequences were uplifted (Liu et al., 1999; Fu, 2005).

Ongoing compression that resulted from the Indian-Asian collision likely drove the dehydration of aquifers and circulation of basinal brines (Hou et al., 2006) that leached the metals from the source rocks to produce the ore-forming fluids (Hu et al., 1998; Tang et al., 2013, 2017; Hu et al., 2013). The metal cations (i.e., Zn^{2+} and Pb^{2+}) were transported mainly

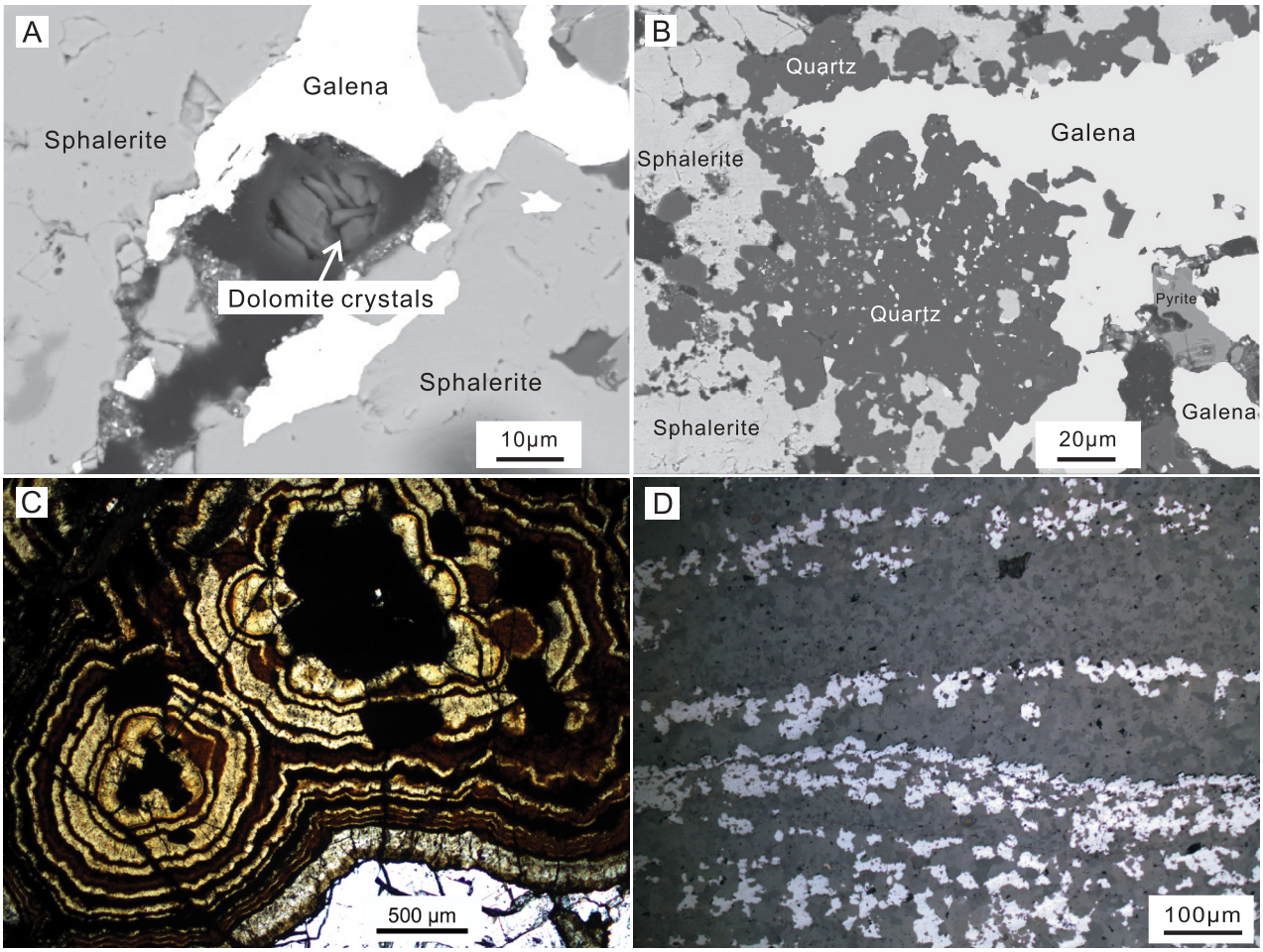

Fig. 16. Backscattered electron image of ores from the Jinding deposit. A. Euhedral dolomite and calcite in a cavity. B. Quartz cement in ores. C. The colloform sphalerite. D. Alternating layers of sulfides parallel to a fissure filling with calcite and bitumen.

as chloride complexes in a fluid that contained no H_2S (Williams-Jones and Migdisov, 2014). These hot metalliferous fluids flowed into the Jinding dome where they mixed with the H_2S-rich hydrocarbon reservoirs and reacted with the H_2S, rapidly precipitating fine-grained sulfides (sphalerite, galena, and pyrite; Fig. 17A, B). The sulfides that precipitated during this stage inherited the ^{34}S-depleted characteristic of MSR-derived hydrogen sulfide.

With further inflow of hot fluid, the system temperature gradually increased to above the temperature at which MSR is possible but also above the minimum temperature required for TSR. Thus, during late mineralization, the TSR-derived H_2S became the main factor to induce metal sulfide precipitation. This explains the elevated $\delta^{34}S$ values (–8 to 0‰) in sphalerite, galena, and pyrite. The hydrocarbons were oxidized to form bitumen residues with higher $\delta^{34}S$ values (–7.38 to –4.61‰) (Fig. 11). The relicts of gypsum dissolution and the abundant sulfate concentration of the fluid inclusions (Luo et al., 1994; Wen et al., 1995) are consistent with late-stage TSR. Owing to the low generation rate of H_2S through TSR, sulfide precipitation proceeded slowly in the form of coarse-grained colloform sphalerite and galena (Figs. 3F, 16C, 17C, D). As H_2S was generated mainly along the hydrocarbon-water interface during TSR, the sulfide minerals could also be precipitated as banded ores in places (Figs. 16D, 17C; Saintilan et al., 2016).

Conclusions

The petrographic characteristics and maturity-related biomarker parameters show that solid bitumen of the Jinding ores had higher thermal maturity than the bitumen of the Sanhedong Formation. In both cases, the bitumen was likely derived from a mixed marine shale and carbonate depositional environment, and the source rocks were most likely the Triassic marine strata in the Lanping basin. It is proposed that MSR occurred in Triassic strata prior to or during migration of hydrocarbon to the Jinding dome, during uplift of these Triassic sequences. The MSR-derived H_2S coexisted with the hydrocarbons in the Jinding dome before mineralization. During the early (main) mineralization stage, Zn- and Pb-bearing hydrothermal fluids flowed into H_2S-rich hydrocarbon reservoirs and rapidly precipitated fine-grained disseminated sphalerite and galena. The hydrocarbons were altered to solid bitumen during subsequent TSR that generated H_2S as a result of the interactions between hydrocarbons, sulfate, and hydrothermal fluid, causing late-stage mineralization.

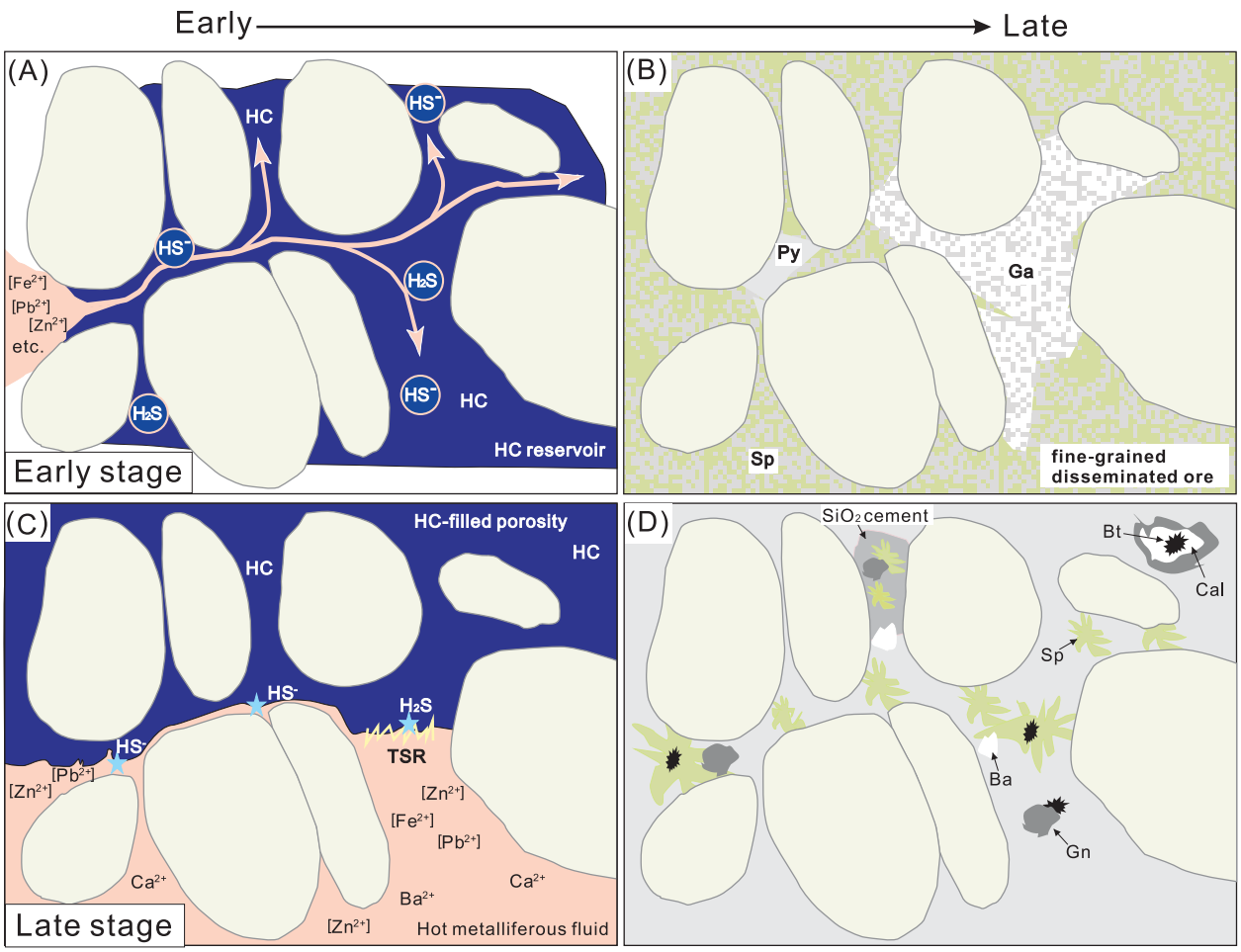

Fig. 17. A metallogenic model for the Jinding Zn-Pb deposit. Parts A and B illustrate the processes that correspond to the early mineralization stage. The hot metalliferous fluid flowed into the Jinding dome and mixed with H_2S-bearing hydrocarbon liquids; fine-grained sulfide minerals precipitated rapidly and disseminated. Parts C and D correspond to the late mineralization stage. C. Thermochemical sulfate reduction occurred at the interface between the HC-filled pores and the hot metalliferous fluid, and H_2S was produced (Machel, 2001; Saintilan et al., 2016). D. The coarse-grained and colloform sphalerite and galena were precipitated. The fluctuation of the hydrocarbon–water interface and formation of H_2S along this interface may explain the alternating layers of sulfides (D). $[Zn^{2+}]$: the square bracket "[ ]" indicates that these metal cations were transported as aqueous chloride complexes. Abbreviations: Ba = barite, Bt = bitumen, Cal = calcite, Ga = galena, HC = hydrocarbon, Py = pyrite, Sp = sphalerite.

Acknowledgments

This research was financially supported by the National Natural Science Foundation of China (41702101, 42072098, 91955209, 41703047), the National Basic Research Program (2015CB452603), the National Key R&D Program of China (2017YFC0602601), and the West Light Foundation of the Chinese Academy of Science. The authors thank Dr. Bin Cheng at the Guangzhou Institute of Geochemistry, Chinese Academy of Science, for his constructive comments on the first draft of the manuscript. We also thank Drs. Williams-Jones and Scott Bohle for their constructive reviews.

REFERENCES

Basuki, N.I., Taylor, B.E., and Spooner, E.T.C., 2008, Sulfur isotope evidence for thermochemical reduction of dissolved sulfate in Mississippi Valley-type zinc-lead mineralization, Bongara Area, Northern Peru: Economic Geology, v. 103, p. 783–799.

Bennett, P.C., 1991, Quartz dissolution in organic-rich aqueous systems: Geochimica et Cosmochimica Acta, v. 55, p. 1781–1797.

Bi, X.W., Tang, Y.Y., Tao, Y., Wang, C.M., Xu, L.L., Qi, H.W., Lan, Q., and Mu, L., 2019, Composite metallogenesis of sediment-hosted Pb-Zn-Ag-Cu base metal deposits in the Sanjiang Collisional Orogen, SW China, and its deep driving mechanism: Acta Petrological Sinica, v. 35, p. 1341–1371.

Blount, C.W., 1977, Barite solubilities and the thermodynamic quantities up to 300 degrees Celsius and 1400 bars: American Mineralogist, v. 62, p. 942–957.

Bray, E.E., and Evans, E.D., 1961, Distribution of n-paraffins as a clue to recognition of source beds: Geochimica et Cosmochimica Acta, v. 22, p. 2–15.

Brunner, B., and Bernasconi, S.M., 2005, A revised isotope fractionation model for dissimilatory sulfate reduction in sulfate reducing bacteria: Geochimica et Cosmochimica Acta, v. 69, p. 4759–4771.

Cai, C., Worden, R.H., Wolff, G.A., Bottrell, S., Wang, D., and Li, X., 2005, Origin of sulfur rich oils and H_2S in Tertiary lacustrine sections of the Jinxian Sag, Bohai Bay basin, China: Applied Geochemistry, v. 20, p. 1427–1444.

Cai, C., Xiang, L., Yuan, Y., Xu, C., He, W., Tang, Y., and Borjigin, T., 2017, Sulfur and carbon isotopic compositions of the Permian to Triassic TSR and non-TSR altered solid bitumen and its parent source rock in NE Sichuan Basin: Organic Geochemistry, v. 105, p. 1–12.

Canfield, D.E., and Teske, A., 1996, Late Proterozoic rise in atmospheric oxygen concentration inferred from phylogenetic and sulfur-isotope studies: Nature, v. 382, p. 127–132.

Canfield, D.E., Farquhar, J., and Zerkle, A.L., 2010, High isotope fractionations during sulfate reduction in a low-sulfate euxinic ocean analog: Geology, v. 38, p. 415–418.

Chen, Y.H., 2015, The sulfur isotopic geochemical characteristics and its metallogeny significance of the Yunnan Jinding lead-zinc deposit: Unpublished M.Sc. thesis, Beijing, China, China University of Geosciences, 49 p. (in Chinese with English abstract).

Chen, Z.H., Cao, Y.C., Wang, X.L., Qiu, L.W., Tang, Y., and Yuan, G.H., 2016, Oil origin and accumulation in the Paleozoic Chepaizi-Xinguang field, Junggar Basin, China: Journal of Asian Earth Science, v. 115, p. 1–15.

Chi, G.X., Xue, C.J., Sun, X.D., Lai, J.Q., Luo, P., Song, H., Li, S., and Zeng, R., 2017, Formation of a giant Zn-Pb deposit from hot brines injecting into a shallow oil-gas reservoir in sandstones, Jinding, southwestern China: Terra Nova, v. 29, p. 312–320.

Cisternas, M.E., and Hermosilla, J., 2006, The role of bitumen in stratabound copper deposit formation in the Copiapo area, Northern Chile: Mineralium Deposita, v. 41, p. 339–355.

Clark, J.R.C., and Blumer, M., 1967, Distribution of n-paraffins in marine organisms and sediments: Limnology & Oceanography, v. 12, p. 79–87.

Dembicki, J.H., Meinschein, W.G., and Hattin, D.E., 1976, Possible ecological and environmental significance of the predominance of even-carbon number C_{20}–C_{30} n-alkanes: Geochimica et Cosmochimica Acta, v. 40, p. 203–208.

Deng, J., Wang, C.M., and Li, G.J., 2012, Style and process of the superimposed mineralization in the Sanjiang Tethys: Acta Petrologica Sinica, v. 28, p. 1349–1361 (in Chinese with English abstract).

Deng, J., Wang, Q., Li, G., and Santosh, M., 2014, Cenozoic tectono-magmatic and metallogenic processes in the Sanjiang region, southwestern China: Earth Science Reviews, v. 138, p. 268–299.

Didyk, B.M., Simoneit, B.R.T., Brassell, S.C., and Eglinton, G., 1978, Organic geochemical indicators of palaeoenvironmental conditions of sedimentation: Nature, v. 272, p. 216–222.

Farrimond, P., Taylor, A., and Telnaes, N., 1998, Biomarker maturity parameters: The role of generation and thermal degradation: Organic Geochemistry, v. 29, p. 1181–1197.

Fu, X.G., 2005, Evolution of Lanping Basin and formation of relevant metal deposits: Journal of Earth Sciences and Environment, v. 27, p. 26–32 (in Chinese with English abstract).

Fu, X.G., Lin, L., Zhu, L.D., Pang, Y.C., and Wang, X.L., 2006, The characteristics of organic matter and its mineralization in the Jinding lead-zinc deposit, Yunnan, China: Journal of Chengdu University of Technology, v. 33, p. 621–630 (in Chinese with English abstract).

Furusaka, C., 1961, Sulphate transport and metabolism desulphovibrio desulphuricans: Nature, v. 192, p. 427–429.

Gao, B.Y., Xue, C.J., Chi, G.X., Li, C., Qu, W.J., Du, A.D., Li, Z.H., and Gu, H., 2012, Re-Os dating of bitumen in the giant Jinding Zn-Pb deposit, Yunnan and its geological significance: Acta Petrologica Sinica, v. 28, p. 1561–1567 (in Chinese with English abstract).

Gao, Y.B., Xue, C.J., and Zeng, R., 2008, Forming mechanisms of H_2S in the Jinding Pb-Zn deposit, Lanping Basin, Northwest Yunnan Province: Journal of Earth Sciences and Environment, v. 30, p. 367–372 (in Chinese with English abstract).

Goldhaber, M.B., and Kaplan, I.R., 1975, Controls and consequences of sulfate reduction rates in recent marine sediments: Soil Science, v. 119, p. 42–55.

Goldhaber, M.B., and Orr, W.L., 1995, Kinetic controls on thermochemical sulfate reduction as a source of sedimentary H_2S: ACS Symposium Series, p. 412–425.

Greenwood, P.F., Brocks, J.J., Grice, K., Schwark, L., Jaraula, C.M.B., Dick, J.M., and Evans, K.A., 2013, Organic geochemistry and mineralogy. I. Characterisation of organic matter associated with metal deposits: Ore Geology Reviews, v. 50, p. 1–27.

Grosjean, E., Love, G.D., Stalvies, C., Fike, D.A., and Summons, R.E., 2009, Origin of petroleum in the Neoproterozoic-Cambrian South Oman salt basin: Organic Geochemistry, v. 40, p. 87–110.

Hanor, J.S., 2000, Barite-celestine geochemistry and environments of formation: Reviews in Mineralogy & Geochemistry, v. 40, p. 193–275.

Hanson, A.D., Zhang, S.C., Moldowan, J.M., Liang, D.G., and Zhang, B.M., 2000, Molecular organic geochemistry of the Tarim Basin, northwest China: AAPG Bulletin, v. 84, p. 1109–1128.

He, L., Song, Y., Chen, K., Hou, Z., Yu, F., Yang, Z., Wei, J., Li, Z., and Liu, Y., 2009, Thrust-controlled, sediment-hosted, Himalayan Zn-Pb-Cu-Ag deposits in the Lanping foreland fold belt, eastern margin of Tibetan Plateau: Ore Geology Reviews, v. 36, p. 106–132.

Hoefs, J., 2004. Stable isotope geochemistry, 5th ed: Berlin, Springer-Verlag, 244 p.

Holba, A.G., Dzou, L.I., Wood, G.D., Ellis, L., Adam, P., Schaeffer, P., Albrecht, P., Greene, T., and Hughes, W.B., 2003, Application of tetracyclic polyprenoids as indicators of input from fresh-brackish water environments: Organic Geochemistry, v. 34, p. 441–469.

Hou, Z., Duan, L., Lu, Y., Zheng, Y., Zhu, D., Yang, Z., Yang, Z., Wang, B., Pei, Y., and Zhao, Z., 2015, Lithospheric architecture of the Lhasa terrane and its control on ore deposits in the Himalayan-Tibetan orogen: Economic Geology, v. 110, p. 1541–1575.

Hou, Z.Q., Pan, G.T., Wang, A.J., Mo, X.X., Tian, S.H., Sun, X.M., Ding, L., Wang, E.Q., Gao, Y.F., Xie, Y.L., Zeng, P.S., Qin, K.Z., Xu, J.F., Qu, X.M., Yang, Z.M., Yang, Z.S., Fei, H.C., Meng, X.J., and Li, Z.Q., 2006, Metallogenesis in Tibetan collisional orogenic belt: II. Mineralization in late-collisional transformation setting: Mineral Deposits, v. 25, p. 521–543 (in Chinese with English abstract).

Hu, G.Y., Li, Y.H., and Zeng, P.S., 2013, The role of Halosalt in mineralization of the Jinding Pb-Zn deposit: Evidence from sulfur and strontium isotope compositions: Acta Geological Sinica, v. 87, p. 1694–1702.

Hu, M.A.,1989, Hydrothermal maturation of indigenous organic matters and their significance in the metallogenic processes of the Jinding Lead-Zinc deposit, Yunnan province: Journal of China University of Geosciences (Earth Science), v. 14, p. 503–512 (in Chinese with English abstract).

Hu, R.Z., Zhong, H., Ye, Z.J., Bi, X.W., Turner, G., and Burnard, P.G., 1998, Helium and argon isotopic geochemistry of Jinding superlarge Pb-Zn deposit: Science in China (Series D), v. 28, p. 208–213 (in Chinese with English abstract).

Huang, D., Zhang, D., and Li, J., 1994, The origin of 4-methyl steranes and pregnanes from Tertiary strata in the Qaidam Basin, China: Organic Geochemistry, v. 22, p. 343–348.

Huang, W.Y., and Meinschein, W.G., 1979, Sterols as ecological indicators: Geochimica et Cosmochimica Acta, v. 43, p. 739–745.

Huang, Z.L., Chen, J., Han, R.S., Li, W.B., Liu, C.Q., Zhang, Z.L., Ma, D.Y., Gao, D.R., and Yang, H.L., 2004, Geochemistry and ore-formation of the Huize giant lead-zinc deposit, Yunnan, China, and Discussion on the Relationship Between Emeishan Flood Basalts and Lead-Zinc Mineralization: Beijing, Geological Publishing House, 1–204 p (in Chinese).

Hughes, W.B., Holba, A.G., and Dzou, L.I.P., 1995, The ratios of dibenzothiophene to phenanthrene and pristane to phytane as indicators of depositional environment and lithology of petroleum source rocks: Geochimica et Cosmochimica Acta v. 59, p. 3581–3598.

Jacob, H., 1989, Classification, structure, genesis and practical importance of natural solid oil bitumen ("migrabitumen"): International Journal of Coal Geology, v. 11, p. 65–79.

Jin, X., Wang, Y., and Xie, G., 2003, Devonian to Triassic Successions of the Changning-Menglian belt, western Yunnan, China: Acta Geologica Sinica (English edition), v. 77, p. 440–456.

Johnston, D.T., Farquhar, J., and Canfield, D.E., 2007, Sulfur isotope insights into microbial sulfate reduction: When microbes meet models: Geochimica et Cosmochimica Acta, v. 71, p. 3929–3947.

Kelemen, S.R., Walters, C.C., Kwiatek, P.J., Afeworki, M., Sansone, M., Freund, H., Pottorf, R.J., Machel, H.G., Zhang, T., Ellis, G.S., Tang, Y., and Peters, K.E., 2008, Distinguishing solid bitumens formed by thermochemical sulfate reduction and thermal chemical alteration: Organic Geochemistry, v. 39, p. 1137–1143.

Kesler, S.E., Jones, H.D., Furman, F.C., Sassen, R., Anderson, W.H., and Kyle, J.R., 1994, Role of crude oil in the genesis of Mississippi Valley-type deposits: Evidence from the Cincinnati arch: Geology, v. 22, p. 609–612.

King, H.E., Walters, C.C., Horn, W.C., Zimmer, M., Heines, M.M., Lamberti, W.A., Kliewer, C., Pottorf, R.J., and Macleod, G., 2014, Sulfur isotope analysis of bitumen and pyrite associated with thermal sulfate reduction in reservoir carbonates at the Big Piney-La Barge production complex: Geochimica et Cosmochimica Acta, v. 134, p. 210–220.

Knauss, K.G., Copenhaver, S.A., Braun, R.L., and Burnham, A.K., 1997, Hydrous pyrolysis of New Albany and Phosphoria shales: Production kinetics of carboxylic acids and light hydrocarbons and interactions between the inorganic and organic chemical systems: Organic Geochemistry, v. 27, p. 477–496.

Kodner, R.B., Pearson, A., Summons, R.E., and Knoll, A.H., 2008, Sterols in red and green algae: Quantification, phylogeny, and relevance for the interpretation of geologic steranes: Geobiology, v. 6, p. 411–420.

Kozłowski, A., 1995, Origin of Zn-Pb ores in the Olkusz and Chrzanów districts: A model based on fluid inclusion: Acta Geologica Polonica, v. 45, p. 84–141.
Kyle, J.R., and Li, N., 2002, Jinding: A giant Tertiary sandstone-hosted Zn-Pb deposit, Yunnan, China: SEG Newsletter, v. 50, p. 8–16.
Leach, D.L., Sangster, D.F., Kelley, K.D., Large, R.R., Garven, G., Allen, C.R., Gutzmer, J., and Walters, S.G., 2005, Sediment-hosted lead-zinc deposit: A global perspective: Economic Geology, v. 100, p. 561–607.
Leach, D.L., and Song, Y.C., 2019, Sediment-hosted zinc-lead and copper deposits in China: Society of Economic Geologists, Special Publication 22, p. 325–409.
Leach, D.L., Song, Y.C., and Hou, Z.Q., 2016, The world-class Jinding Zn-Pb deposit: Ore formation in an evaporite dome, Lanping basin, Yunnan, China: Mineralium Deposita, v. 52, p. 281–296.
Leventhal, J.S., 1990, Organic matter and thermochemical sulfate reduction in the Viburnum Trend, Southeast Missouri: Economic Geology, v. 85, p. 622–632.
Li, X.M., and Song, Y.G., 2006, Cenozoic evolution of tectono-fluid and metallogenic process in Lanping Basin, western Yunnan Province, Southwest China: Constraints from apatite fission track data: Chinese Journal of Geochemistry, v. 25, p. 395–400.
Liu, D.Z., Tao X.F., and Zhu, L.D., 1999, The coupling relationship between basin and mountain building in Lanping basin, northwestern Yunnan province: Chengdu, Southwest Jiaotong University Press, 1–175 p. (in Chinese).
Liu, J.L., Song, Z.J., Gao, S.Y., Zhai, Y.F., Wang, A.J., Gao, L., Xiu, Q.Y., and Cao, D.H., 2006, The dynamic setting and processes of tectonic and magmatic evolution of the oblique collision zone between Indian and Eurasian plates: Exemplified by the tectonic evolution of the Three River Region, eastern Tibet: Acta Petrologica Sinica, v. 22, p. 775–786 (in Chinese with English abstract).
Luo, J.L., Yang, Y.H., Zhao, Z., Chen, J.S., and Yang, J.Z., 1994, Evolution of the Tethys in western Yunnan and mineralization for main metal deposits: Beijing, Geological Publishing House, 157–215 p. (in Chinese with English abstract).
Machel, H.G., 1987a, Saddle dolomite as a by-product of chemical compaction and thermochemical sulfate reduction: Geology, v. 15, p. 936–940.
——1987b, Some aspects of diagenetic sulphate-hydrocarbon redox reactions: Geological Society London Special Publications, v. 36, p. 15–28.
—— 2001, Bacterial and thermochemical sulfate reduction in diagenetic settings—old and new insights: Sedimentary Geology, v. 140, p. 143–175.
Machel, H.G., Krouse, H.R., and Sassen, R., 1995, Products and distinguishing criteria of bacterial and thermochemical sulfate reduction: Applied Geochemistry, v. 10, p. 373–389.
Mackenzie, A.S., and McKenzie, D., 1983, Isomerization and aromatization of hydrocarbons in sedimentary basins formed by extension: Geological Magazine, v. 120, p. 417–470.
Manning, D.A.C., and Gize, A.P., 1993, The role of organic matter in ore transport processes, *in* Engels, M.H., and Macko, S.A., eds., Organic geochemistry: Principles and applications: New York, Plenum Press, p. 547–563.
Metcalfe, I., 2013, Gondwana dispersion and Asian accretion: Tectonic and palaeogeographic evolution of eastern Tethys: Journal of Asian Earth Sciences, v. 66, p. 1–33.
Orr, W.L., 1977, Geologic and geochemical controls on the distribution of hydrogen sulfide in natural gas: Advances in Organic Geochemistry, Enadisma, Madrid, p. 571–597.
Peters, K.E., and Moldowan, J.M., 1993, The biomarker guide: Interpreting molecular fossils in petroleum and ancient sediments: New York, Prentice Hall Inc., 1–178 p.
Peters, K.E., Walters, C.C., and Moldowan, J.M., 2005, The biomarker guide: Cambridge, Cambridge University Press.
Picard, A., Gartman, A., Clarke, D.R., and Girguis, P.R., 2018, Sulfate-reducing bacteria influence the nucleation and growth of mackinawite and greigite: Geochimica et Cosmochimica Acta, v. 220, p. 367–384.
Powell, T.G., and Macqueen, R.W., 1984, Precipitation of sulfide ores and organic matter: Sulfate reactions at Pine Point, Canada: Science, v. 224, p. 63–66.
Püttmann, W., Hagemann, H.W., Merz, C., and Speczik, S., 1988, Influence of organic material on mineralization processes in the Permian Kupferschiefer Formation, Poland: Organic Geochemistry, v. 13, p. 357–363.
Qin, G.J., and Zhu, S.Q., 1991, Genetic model and prospecting prediction of Jinding lead-zinc ore deposit: Yunnan Geology, v. 10, p. 145–190 (in Chinese with English abstract).
Radke, M., 1988, Application of aromatic compounds as maturity indicators in source rocks and crude oils: Marine Petroleum Geology, v. 5, p. 224–236.
Radke, M., and Welte, D.H., 1983, The methylphenanthrene index (MPI): A maturity parameter based on aromatic hydrocarbons, *in* Bjorøy, M., et al., eds., Advances in organic geochemistry: Chichester: Wiley, p. 224–237.
Radke, M., Welte, D.H., and Willsch, H., 1982, Geochemical study on a well in the Western Canada Basin: Relation of the aromatic distribution pattern to maturity of organic matter: Geochimica et Cosmochimica Acta, v. 46, p. 1–10.
Radke, M., Welte, D.H., and Willsch, H., 1986, Maturity parameters based on aromatic hydrocarbons: Influence of the organic matter type: Organic Geochemistry, v. 10, p. 51–63.
Requejo, A.G., Hieshima, G.B., Hsu, C.S., McDonald, T.J., and Sassen, R., 1997, Short chain (C_{21} and C_{22}) diasteranes in petroleum and source rocks as indicators of maturity and depositional environments: Geochimica et Cosmochimica Acta, v. 61, p. 2653–2667.
Rieger, A., Schwark, L., Cisternas, M.E., and Miller, H., 2008, Genesis and evolution of bitumen in Lower Cretaceous lavas and implications for strata-bound copper deposits, North Chile: Economic Geology, v. 103, p. 387–404.
Rontani, J.F., and Volkman, J.K., 2003, Phytol degradation products as biogeochemical tracers in aquatic environments: Organic Geochemisty, v. 34, p. 1–35.
Rullkötter, J., and Marzi, R., 1988, Natural and artificial maturation of biological markers in a Toarcian shale from northern Germany: Organic Geochemistry, v. 13, p. 639–645.
Rybicki, M., Marynowski, L., Stukins, S., Nejbert, K., 2017, Age and origin of the well-preserved organic matter in internal sediments from the Silesian-Cracow lead-zinc deposits, Southern Poland: Economic Geology, v. 112, p. 775–798.
Saintilan, N.J., Spangenberg, J.E., Chiaradia, M., Chelle-Michou, C., Stephens, M.B., and Fontboté, L., 2015, Source and role of exogenous hydrocarbons at the Mississippi Valley-type Pb-Zn mineralisation at Laisvall, Sweden [ext. abs.]: International Meeting on Organic Geochemistry, Prague, 2015, Extended Abstracts, p. 382–383.
Saintilan, N.J., Spangenberg, J.E., Samankassou, E., Kouzmanov, K., Chiaradia, M., Stephens, M.B., and Fontboté, L., 2016, A refined genetic model for the Laisvall and Vassbo Mississippi Valley-type sandstone-hosted deposits, Sweden: Constraints from paragenetic studies, organic geochemistry, and S, C, N and Sr isotope data: Mineralium Deposita, v. 51, p. 639–664.
Schoonen, M.A., 2004, Mechanisms of sedimentary pyrite formation: Special Paper of the Geological Society of America, no. 379, p. 117–134.
Seifert, W.K., and Moldowan, J.M., 1986, Use of biological markers in petroleum exploration: Methods in Geochemistry and Geophysics, v. 24, p. 261–290.
Shanmungam, G., 1985, Significance of coniferous rain forests and related organic matter in generating commercial quantities of oil, Gippsland Basin, Australia: AAPG Bulletin, v. 69, p. 1241–1254.
Sim, M.S., Bosak, T., and Ono, S., 2011, Large sulfur isotope fractionation does not require disproportionation: Science, v. 333, p. 74–77.
Sinninghe Damst´e, J.S., and de Leeuw, J.W., 1990, Analysis, structure and geochemical significance of organically bound sulfur in the geosphere: State of the art and future research: Organic Geochemistry, v. 16, p. 1077–1101.
Song, Y.C., Hou, Z.Q., Xue, C.D., and Huang, S.Q., 2020, New mapping of the world-class Jinding Zn-Pb deposit, Lanping basin, Southwest China: Genesis of ore host rocks and records of hydrocarbon-rock interaction: Economic Geology, v. 115, p. 981–1002.
Song, Y.C., Liu, Y.C., Hou, Z.Q., Fard, M., Zhang, H.R., and Zhuang, L.L., 2019, Sediment-hosted Pb-Zn deposits in the Tethyan domain from China to Iran: Characteristics, tectonic setting, and ore controls: Gondwana Research, v. 75, p. 249–281.
Spangenberg, J.E., and Herlec, U., 2006, Hydrocarbon biomarkers in the Topla-Mežica zinc-lead deposits, northern Karavanke/Drau Range, Slovenia: Paleoenvironment at the site of ore formation: Economic Geology, v. 101, p. 997–1021.
Spangenberg, J.E., and Macko, S.A., 1998, Organic geochemistry of the San Vicente zinc-lead district, eastern Pucará Basin, Peru: Chemical Geology, v. 146, p. 1–23.
Summons, R.E., Hope, J.M., Swart, R., and Walter, M.R., 2008, Origin of Nama basin bitumen seeps: Petroleum derived from a Permian lacustrine source rock traversing southwestern Gondwana: Organic Geochemistry, v. 39, p. 589–607.
Tang, Y.Y., Bi, X.W., Wu, L.Y., Zou, Z.C., and He, L.P., 2013, Carbon, oxygen, strontium and lead isotopic geochemistry in the Jinding super-large Zn-Pb

deposit, Yunnan Province: Geochimica, v. 42, p. 467–480 (in Chinese with English abstract).

Tang, Y.Y., Bi, X.W., Fayek, M., Hu, R.Z., Wu, L.Y., Zou, Z.C., Feng, C.X., and Wang, X.S., 2014, Microscale sulfur isotopic compositions of sulfide minerals from the Jinding Zn-Pb deposit, Yunnan Province, Southwest China: Gondwana Research, v. 26, p. 594–607.

Tang, Y.Y., Bi, X.W., Fayek, M., Stuart, F.M., Wu, L.Y., Jiang, G., Xu, L., and Liang, F., 2017, Genesis of the Jinding Zn-Pb deposit, northwest Yunnan Province, China: Constraints from rare earth elements and noble gas isotopes: Ore Geology Reviews, v. 90, p. 970–986.

Third Geological Team, 1984, The Jinding Pb-Zn deposit. Exploration Report, Lanping County, Yunnan Province: Yunnan Bureau of Geology and Mineral Resources, Yunnan, 101–105 p. (in Chinese).

Toland, W.G., 1960, Oxidation of organic compounds with aqueous sulfate: Journal of the American Chemical Society, v. 82, p. 1911–1916.

Volkman, J.K., Barrett, S.M., Dunstan, G.A., and Jeffrey, S.W., 1994, Sterol biomarkers for microalgae from the green algal class *Prasinophyceae*: Organic Geochemistry, v. 21, p. 1211–1218.

Volkman, J.K., Barrett, S.M., Blackburn, S.I., Mansour, M.P., Sikes, E.L., and Gelin, F.O., 1998, Microalgal biomarkers: A review of recent research developments: Organic Geochemistry, v. 29, p. 1163–1179.

Volkman, J.K., Barrett, S.M., and Blackburn, S.I., 1999, Eustigmatophyte microalgae are potential sources of C_{29} sterols, C_{22}-C_{28} n-alcohols and C_{28}-C_{32} n-alkyl diols in freshwater environments: Organic Geochemistry, v. 30, p. 307–318.

Wang, A.J., Cao, D.H., Gao, L., Wang, G.S., Guan, Y., Xiu, Q.Y., and Liu, J.L., 2009, A probe into the genesis of Jinding super-large lead-zinc ore deposit: Acta Geologica Sinica, v. 83, p. 43–54 (in Chinese with English abstract).

Wang, C., Bagas, L., Lu, Y., Santosh, M., Du, B., and McCuaig, T.C., 2016, Terrane boundary and spatio-temporal distribution of ore deposits in the Sanjiang Tethyan Orogen: Insights from zircon Hf-isotopic mapping: Earth-Science Reviews, v. 156, p. 39–65.

Wang, D.R., and Zhang, K., 2003, The oil and gas potential of the Cenozoic basin in Yunnan province: Beijing, Geological House, 1–171 p. (in Chinese).

Wang, G., Wang, T.G., Simoneit, B., Zhang, L., and Zhang, X., 2010, Sulfur rich petroleum derived from lacustrine carbonate source rocks in Bohai Bay Basin, East China: Organic Geochemistry, v. 41, p. 340–354.

Wang, Z., 2013, The ore-forming fluid and mineralization mechanism in super giant Jinding lead-zinc deposit: Unpublished M.Sc. thesis, Beijing, China, China University of Geosciences, 1–91 p.

Waples, D.W., and Machihara, T., 1991, Biomarkers for geologists–A practical guide to the application of steranes and triterpanes in petroleum geology: American Association of Petroleum Geologists, AAPG Bulletin, Method Exploration Series 9, 85 p.

Wen, C.Q., Cai, J.M., Liu, W.Z., Qin, G.J., and Chen, S.F., 1995, Geochemical characteristics of fluid inclusions in the Jinding lead-zinc deposit, Yunnan, China: Journal of Mineralogy and Petrology, v. 15, p. 78–84 (in Chinese with English abstract).

Williams-Jones, A.E., and Migdisov, A.A., 2014, Experimental constraints and deposition of metals in ore-forming hydrothermal systems: Society of Economic Geologists Special Publication 18, p. 77–95.

Williford, K.H., Grice, K., Logan, G.A., Chen, J., and Huston, D., 2011, The molecular and isotopic effects of hydrothermal alteration of organic matter in the Paleoproterozoic McArthur River Pb/Zn/Ag ore deposit: Earth and Planetary Science Letters, v. 301, p. 382–392.

Wilson, N.S.F., Stasiuk, L.D., and Fowler, M.G., 2007, Origin of organic matter in the Proterozoic Athabasca Basin of Saskatchewan and Alberta, and significance to unconformity uranium deposits: Bulletin of the Geological Survey of Canada, 325–339 p.

Wing, B.A., and Halevy, I., 2014, Intracellular metabolite levels shape sulfur isotope fractionation during microbial sulfate respiration: Proceedings of the National Academy of Sciences, v. 111, p. 18,116–18,125.

Wingert, W., and Pomerantz, M., 1986, Structure and significance of some twenty-one and twenty-two carbon petroleum steranes: Geochimica et Cosmochimica Acta, v. 50, p. 2763–2769.

Worden, R.H., and Cai, C., 2006, Geochemical characteristics of the Zhaolanzhuang sour gas accumulation and thermochemical sulfate reduction in the Jixian Sag of Bohai Bay Basin by Zhang et al. (Organic Geochemistry 36, 1717–1730): Organic Geochemistry, v. 37, p. 511–514.

Worden, R.H., Smalley, P.C., and Oxtoby, N.H., 1995, Gas souring by thermochemical sulfate reduction at 140°C: American Association of Petroleum Geologists Bulletin, v. 79, p. 854–863.

Wu, G.G., and Wu, X.D., 1989, A preliminary study on the tectonic evolution and mineralisation regularity of the Jinding lead-zinc deposit, Yunnan province: Earth Science, v. 14, p. 477–486 (in Chinese with English abstract).

Xiao, H., Li, M.J., Yang, Z., and Zhu, Z.L., 2019, Distribution patterns and geochemical implications of C19-C23 tricyclic terpanes in source rocks and crude oils occurring in various depositional environments: Geochimica, v. 48, p. 161–170 (in Chinese with English abstract).

Xue, C.J., Chen, Y.C., Yang, J.M., and Wang, D.H., 2002, Analysis of ore-forming background and tectonic system of Lanping basin, Western Yunnan Province: Mineral Deposits, v. 21, p. 36–44 (in Chinese with English abstract).

Xue, C.J., Chen, Y.C., Wang, D.H., Yang, J.M., Yang, W.G., and Zeng, R., 2003, Geology and isotopic composition of helium, neon, xenon and metallogenic age of the Jinding and Baiyangping ore deposits, northwest Yunnan, China: Science in China (Series D), v. 33, p. 315–322 (in Chinese with English abstract).

Xue, C.J., Zeng, R., Liu, S., Chi, G., Qing, H., Chen, Y., Yang, J., and Wang, D., 2007a, Geologic, fluid inclusion and isotopic characteristics of the Jinding Zn-Pb deposit, western Yunnan, South China: A review: Ore Geology Reviews, v. 31, p. 337–359.

Xue, C.J., Gao, Y.B., Zeng, R., Chi, G.X., and Qing, H.R., 2007b, Organic petrography and geochemistry of the giant Jinding deposit, Lanping basin, northwestern Yunnan, China: Acta Petrologica Sinica, v. 23, p. 2889–2900 (in Chinese with English abstract).

Xue, C.J., Gao, Y.B., Chi, G.X., and Leach, D.L., 2009, Possible former oil-gas reservoir in the giant Jinding Pb-Zn Deposit, Lanping, NW-Yunnan: The role in the ore accumulation: Journal of Earth Sciences and Environment, v. 31, p. 221–229 (in Chinese with English abstract).

Xue, C.J., Chi, G., and Fayek, M., 2015, Micro-textures and in situ sulfur isotopic analysis of spheroidal and zonal sulfides in the giant Jinding Zn-Pb deposit, Yunnan, China: Implications for biogenic processes: Journal of Asian Earth Sciences, v. 103, p. 288–304.

Ye, Q.T., Hu, Y.Z., and Yang, Y.Q., 1992, Regional geochemistry background and the gold-silver-lead-zinc mineralization in Sanjiang area: Geological Publishing House, Beijing, 21–264 p. (in Chinese).

Yin, H.H., Fan, W.M., and Lin, G., 1990, Deep factors on the Lanping-Simao basin evolution and the mantle-crust complex mineralization: Tectonic and Metallogeny, v. 4, p. 113–124 (in Chinese with English abstract).

Yuan, B., Mao, J.W., Yan, X.H., Wu, Y., Zhang, F., and Zhao, L.L., 2014, Sources of metallogenic materials and metallogenic mechanism of Daliangzi Ore Field in Sichuan Province: Constraints from geochemistry of S, C, H, O, Sr isotope and trace element in sphalerite: Acta Petrologica Sinica, v. 30, p. 209–220.

Zeng, R., 2007, The Large Scale Fluid Ore-forming Process in the Lanping Basin-taking the Jinding and Baiyangping Deposits as the Examples: Unpublished M.Sc. thesis, Xi'an, China, Chang'an University, 109 p. (in Chinese with English abstract).

Zhang, C.J., Ni, S.J., Ten, Y.G., Peng, X.H., and Liu, J.D., 2000, Relationship between Himalayan Tectonomagmatic movement and mineralization in Lanping basin, Yunnan province: Journal of Mineralogy and Petrology, v. 20, p. 35–39 (in Chinese with English abstract).

Zhang, S.C., Shuai, Y.H., He, K., and Mi, J.K., 2012, Research on the initiation mechanism of thermochemical sulfate reduction (TSR): Acta Petrologica Sinica, v. 28, p. 739–748 (in Chinese with English abstract).

Zhang, Z.B., 2018, Geochemical characteristics of evaporites and its relation to metallogenesis in Lanping basin: Unpublished M.Sc. thesis, Jiangxi, China, East China University of Technology, 85 p.

Zhou, J.X., Huang, Z.L., Zhou, M.F., Zhu, X.K., and Muchez, P., 2014, Zinc, sulfur and lead isotopic variations in carbonate-hosted Pb-Zn sulfide deposits, southwest China: Ore Geology Reviews, v. 58, p. 41–54.

Zhou, W.Q., and Zhou Q.L., 1992, A study on the isotopic composition of Pb and S in the Lanping Pb-Zn deposit, Yunnan province: Geochimica, v. 20, p. 141–148 (in Chinese with English abstract).

Qing Lan is an associate researcher from Institute of Geochemistry, Chinese Academy of Sciences, China. He earned his Ph.D. in structural geology from Guangzhou Institute of Geochemistry, Chinese Academy of Sciences, in 2015. His focus is on the Zn-Pb deposits from the Sanjiang Tethyan tectonic belt. He combines field relationships, petrography, mineralogy, and geochemistry to understand the evolution of ore-forming fluid and origin of deposit.